Influence of the Lode parameter and the stress triaxiality on the failure of elasto-plastic porous materials

K. Danas [a,*], P. Ponte Castañeda [b,c]

[a] Laboratoire de Mécanique des Solides, C.N.R.S. UMR7649, École Polytechnique, 91128 Palaiseau Cedex, France
[b] Department of Mechanical Engineering and Applied Mechanics, University of Pennsylvania, Philadelphia, PA 19104-6315, USA
[c] Madrid Institute for Advanced Studies of Materials (IMDEA-Materials), 28040 Madrid, Spain

ABSTRACT

This work makes use of a recently developed "second-order" homogenization model to investigate failure in porous elasto-plastic solids under general triaxial loading conditions. The model incorporates dependence on the porosity and average pore shape, whose evolution is sensitive to the stress triaxiality and Lode parameter L. For positive triaxiality (with overall tensile hydrostatic stress), two different macroscopic failure mechanisms are possible, depending on the level of the triaxiality. At high triaxiality, void growth induces softening of the material, which overtakes the intrinsic strain hardening of the matrix phase, leading to a maximum in the effective stress–strain relation for the porous material, followed by loss of ellipticity by means of dilatant shear localization bands. In this regime, the ductility decreases with increasing triaxiality and is weakly dependent on the Lode parameter, in agreement with earlier theoretical analyses and experimental observations. At low triaxiality, however, a new mechanism comes into play consisting in the abrupt collapse of the voids along a compressive direction (with small, but finite porosity), which can dramatically soften the response of the porous material, leading to a sudden drop in its load-carrying capacity, and to loss of ellipticity of its incremental constitutive relation through localization of deformation. This low-triaxiality failure mechanism leads to a reduction in the ductility of the material as the triaxiality decreases to zero, and is highly dependent on the value of the Lode parameter. Thus, while no void collapse is observed at low triaxiality for axisymmetric tension ($L = -1$), the ductility of the material drops sharply with decreasing values of the Lode parameter, and is smallest for biaxial tension with axisymmetric compression ($L = +1$). In addition, the model predicts a sharp transition from the low-triaxiality regime, with increasing ductility, to the high-triaxiality regime, with decreasing ductility, as the failure mechanism switches from void collapse to void growth, and is in qualitative agreement with recent experimental work.

© 2012 Elsevier Ltd. All rights reserved.

1. Introduction

Due to its critical technological importance, ductile failure and fracture of metallic materials has been the focus of continued attention over the last sixty years. The main mechanism for material failure in ductile solids is the nucleation, growth and eventual coalescence of voids and micro-cracks as a result of the applied loading conditions (Garrison and Moody, 1987). It has been known for many years that the stress triaxiality, denoted here by X_Σ and defined as the ratio of the mean stress to the von Mises equivalent or effective deviatoric stress, is the critical parameter controlling ductile failure at high triaxiality. Thus, large amounts of experimental data (Hancock and Mackenzie, 1976; Le Roy et al., 1981;

Johnson and Cook, 1985) have shown a monotonic decrease of material ductility with increasing stress triaxiality. This is consistent with the expected increase in the rate of growth of the voids with a larger tensile hydrostatic stress component. Nonetheless, recent experimental evidence (Bao and Wierzbicki, 2004; Barsoum and Faleskog, 2007a; Mohr and Ebnoether, 2009; Dunand and Mohr, 2010) suggests that a new, different mechanism should come into play at low triaxialities, leading to a substantial reduction of the material ductility with *decreasing* stress triaxiality. Indeed, in these studies, it has been found that a second loading parameter, the Lode parameter, L (or equivalently Lode angle, θ) also plays a significant role in ductile failure at low stress triaxialities. The Lode parameter is a function of the third invariant of the stress deviator and is used to distinguish between the different shear stress states in three dimensions (3-D), ranging from axisymmetric tension to biaxial tension with axisymmetric compression and passing through in-plane shear. The key experimental observa-

tions are summarized in Fig. 1, which is taken from the work of Barsoum and Faleskog (2007a). Specifically, Fig. 1a shows the low-triaxiality regime with increasing ductility as the triaxiality increases, followed by an abrupt transition to the standard high-triaxiality regime with the opposite trend. Correspondingly, Figs. 1b–d show SEM micrographs of the failure surfaces for low, intermediate and high triaxiality. At low stress triaxialities (Fig. 1(b)), the dimples are shallow and elongated suggesting significant shear plastic strains and void elongation, together with shear localization between voids. At high stress triaxialities (Fig. 1(d)), the dimples are deep suggesting the well-known void coalescence mechanism with necking of inter-void ligaments leading to final rupture. At an intermediate value of the stress triaxiality ($X_\Sigma \approx 0.7 - 0.8$), a transition between the void shearing and void growth mechanisms is observed. In conclusion, these careful experimental observations strongly suggest that, void elongation (with significant changes in shape), which is dependent on the specific shear stress state (as measured by the Lode parameter), becomes the dominant mechanism leading to the failure of the material at low stress triaxialities, and should therefore be accounted for in the constitutive modeling of such material systems.

The underlying microstructural mechanism at large triaxialities (i.e., large mean stresses compared to the deviatoric ones) was identified early on by McClintock (1968) and Rice and Tracey (1969), who related it to the growth of pre-existing voids or/and nucleated micro-voids mainly due to the presence of impurities in the material. This knowledge led to the development of the well-known Gurson (1977) model (and its modifications by Tvergaard (1981)) which is based on a micromechanical analysis of a spherical shell, assumed to remain spherical even for general loading conditions. However, while this assumption is entirely consistent with the void growth mechanisms observed under pure hydrostatic stress states, as already noted, it becomes less adequate with the addition of shear loads, since such loads can induce significant changes in the void shape. Early studies of the effect of triaxiality on void growth, accounting for shape changes, as well as its implications for ductile failure, were carried out by McClintock (1968, 1971) and Budiansky et al. (1982) (see also Teirlinck et al., 1988). Building on these early works and on the works of Duva and Hutchinson (1984) and Lee and Mear (1992), Gologanu et al. (1993, 1994) proposed a model for porous materials with aligned spheroidal voids that are subjected to axisymmetric stress states aligned with the voids symmetry axis. These Gurson-type models have been further developed by Gologanu et al. (1997), Garajeu et al. (2000), Pardoen and Hutchinson (2000), Benzerga (2002), Flandi and Leblond (2005), Monchiet et al. (2007), Benzerga and
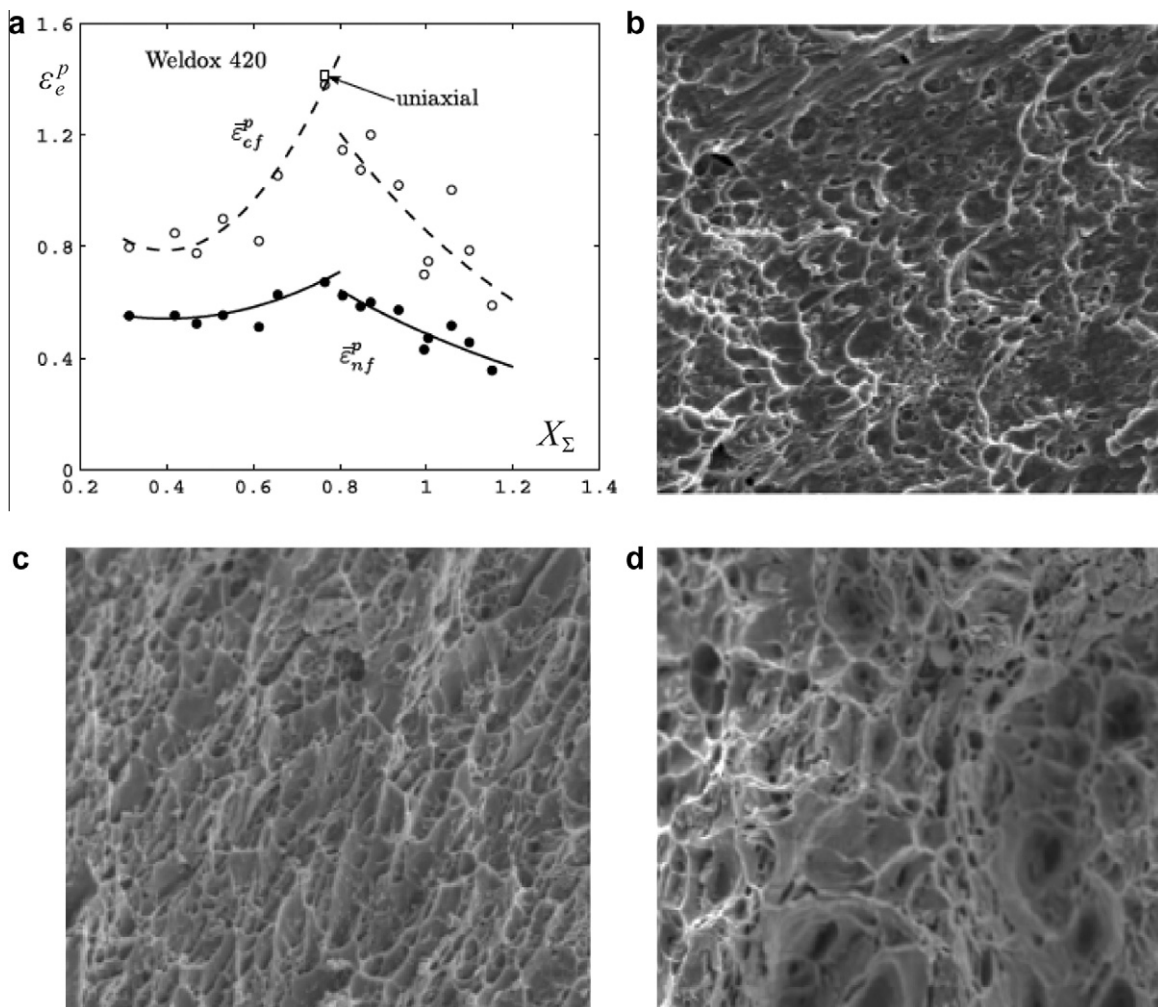
Fig. 1. Failure of hot rolled medium-strength steel. (a) Effective plastic strain and failure vs. stress triaxiality. (On the plot, $\bar{\varepsilon}^p_{cf}$ and $\bar{\varepsilon}^p_{nf}$ refer to the critical plastic strains at the center of a notch and the average plastic strain at the notch, respectively.) The rest of the figures correspond to SEM fractographs showing the rupture modes: (b) a shear dimple rupture mode with inter-void shearing mechanism and elongated voids for stress triaxiality $X_\Sigma = 0.47$; (c) the transition between shear dimples and void growth rupture for $X_\Sigma = 0.85$; (d) necking of inter-void ligaments, i.e., void coalescence due to void growth, for $X_\Sigma = 1.10$. All figures are taken from Barsoum and Faleskog (2007a) and correspond to Weldox 420.

Leblond (2010) and Keralavarma and Benzerga (2010) to account for more general loading conditions (and anisotropic matrix behavior in the case of Keralavarma and Benzerga (2010)), but still make the rather strong approximation that the voids remain *spheroidal* in shape for general triaxial loading histories.

A different class of constitutive models for porous porous viscoplastic materials capable of accounting for more general (i.e., arbitrary ellipsoidal) pore shape and orientation evolution have been developed by Ponte Castañeda and Zaidman (1994), Kailasam et al. (1997a) and Kailasam and Ponte Castañeda (1997) to deal with completely general, three-dimensional loading conditions. These models make use of the "variational linear comparison" homogenization method of Ponte Castañeda (1991) (see also Willis, 1991; Michel and Suquet, 1992), together with the estimates of Ponte Castañeda and Willis (1995) for porous linear-elastic materials with "ellipsoidal" microstructures (i.e., particulate microstructures containing orthotropic distributions of ellipsoidal pores), to generate corresponding estimates for the dissipation potential of the viscoplastic porous materials. They are supplemented by evolution laws for microstructural variables corresponding to the porosity, average pore shape and orientation, which are obtained from the homogenization analyses in a self-consistent fashion (Ponte Castañeda and Zaidman, 1994; Kailasam and Ponte Castañeda, 1998).

The above-mentioned non-linear homogenization methods have also been extended to include strain hardening elasto-plastic behavior for the matrix material, and implemented numerically in large-scale, structural finite element programs by Kailasam et al. (2000) and Aravas and Ponte Castañeda (2004). While these models are quite general, they tend to give overly stiff predictions at high triaxialities (i.e., they are quite a bit stiffer than the Gurson-based models), especially for small porosity levels. However, this limitation has been removed, at least for isotropic matrix systems, in recent work by Danas and Ponte Castañeda (2009a), Danas and Ponte Castañeda (2009b), making use of the more accurate "second-order" linear comparison homogenization method of Ponte Castañeda (2002a), Ponte Castañeda (2002b), and building on earlier works by Danas et al. (2008a), Danas et al. (2008b) and Danas (2008). The resulting model, which will be referred to here as the SOM model, will be extended to account for strain-hardening, elasto-plastic behavior for the matrix phase, and will be capable of handling general "ellipsoidal" particulate microstructures and general three-dimensional loading conditions, including those leading to pore rotation, while remaining quite accurate at large stress triaxialities and recovering the Gurson model for purely hydrostatic loadings and spherical pores.

Application of the linear comparison constitutive models to various types of loading conditions has revealed the importance of void shape evolution in determining the overall response of plastic porous solids. For example, it was found by Ponte Castañeda and Zaidman (1994) that under uniaxial tension the softening induced by the growth of porosity associated with the Gurson model for ideally plastic porous materials is overpowered by pore shape changes, since the pore elongation in the tensile direction provides a hardening mechanism resulting in overall hardening for the porous material—in agreement with numerical simulations (see Kailasam et al. (1997b)). However, the evolution of the void shape can also induce overall softening of the porous material, and in fact it was shown by Ponte Castañeda and Zaidman (1994), and confirmed by Danas and Ponte Castañeda (2009b), that a porous rigid ideally plastic material could even lose ellipticity by *void collapse* leading to shear band formation at low triaxialities. It is important to emphasize that such an effect could not be captured by the Gurson model, since at low-triaxiality conditions the source of the instability cannot be identified with a void growth mechanism (Yamamoto, 1978). In this context, it should also be mentioned that Nahshon and Hutchinson (2008) have proposed an *ad hoc*

modification of the Gurson model in an attempt to account for softening of the material at low stress triaxialities. While, by construction, this modification brings in an effect of the Lode parameter, it is inconsistent with mass conservation, and still fails to account for the development of morphological anisotropy associated with pore shape changes.

Motivated by the above observations, in the present work, we will make use of the SOM model to investigate the influence of the Lode parameter (i.e., the different shear stress states) and the stress triaxiality on the overall behavior of porous elasto-plastic materials and the possible development of "macroscopic" instabilities (Geymonat et al., 1993) due to the evolution of the underlying microstructure, e.g., void growth and void shape changes. In particular, we will consider two possible failure mechanisms for the porous medium: (i) the existence of a limit load (i.e., a maximum point on the effective stress–strain curve or equivalently zero material hardening rate) and (ii) loss of ellipticity of the incremental response leading to localization of deformation in dilatant shear bands, as discussed originally by Rice (1976). It should be noted in this connection that while loss of ellipticity calculations will lead to predictions that are typically on the high side when compared to experimental results, these are *material* instabilities which can provide useful information about the *theoretical* load-carrying capacity of the material. In actual experiments, the loading conditions and specimen geometry will invariably lead to non-uniform fields, such that the instabilities nucleate at critical locations in the specimen where the local fields are in excess of the applied average fields, leading to progressive failure of the material by propagation of the instability into the specimen.

In this work, we will not attempt to model specific experimental conditions, nor structural geometries. However, it is relevant to note that, based on the earlier variational model of Ponte Castañeda and Zaidman (1994), constitutive user-material subroutines for implementation in finite element codes have been developed by Kailasam and Ponte Castañeda (1997), Kailasam et al. (2000) and Aravas and Ponte Castañeda (2004). Recently, Danas and Aravas (2012) have proposed a modification of these earlier models in accord with the present SOM model that recovers the spherical shell solution (i.e., Gurson's hydrostatic point) at purely hydrostatic loadings, while including all the advanced features of the variational and second-order methods such as arbitrary ellipsoidal void shapes and general loading conditions. In addition, in this work we will not address "microscopic" coalescence criteria (see Benzerga et al. (1999), Benzerga and Leblond (2010) for details on this alternative approach to material failure). It should be remarked in this connection that the incorporation of loss of ellipticity predictions into numerical simulations of actual structural problems (including crack propagation) is a challenging and still largely open problem, which is also beyond the scope of this work.

For clarity and simplicity, in our analysis we will consider purely triaxial loading conditions and initially spherical voids so that the void orientation vectors remain aligned with the principal loading conditions for the entire deformation process and therefore do not contribute to the overall material response. Note, however, that for the case of general (non triaxial) loading conditions or initially anisotropic microstructures (i.e., initially ellipsoidal voids misaligned with the laboratory frame axes), the void orientation vectors evolve due to finite deformations and could hence affect the overall response of the porous material (e.g. Kailasam and Ponte Castañeda (1997), Kailasam et al. (2000), Aravas and Ponte Castañeda (2004), Danas and Ponte Castañeda (2009b)). The investigation of void rotation effects in this context will be left for future work, but it should be mentioned that recent numerical studies by Barsoum and Faleskog (2007b) and Tvergaard (2009) have shown that rotation and elongation of the voids along the

shearing direction can contribute to the localization of deformation and subsequent failure of the material.

The rest of the paper is organized as follows. First, in Section 2, we describe the geometry and loading conditions, and define the pertinent variables used in this study including the stress triaxiality and the Lode parameter. In this section, we also describe the microstructure and present a brief summary of the SOM model, as well as the characterization of the limit load and localization conditions used in this study as failure criteria for the porous medium. Then, Section 3 discusses the results obtained by the SOM for the evolution of the stress and the underlying microstructure under finite deformations, and compares them with the (isotropic) modified Gurson model of Nahshon and Hutchinson (2008), referred to as MGUR below. Limit load and localization maps are constructed as a function of the stress triaxiality and the Lode parameter. A parametric study to investigate the influence of the material hardening rate and initial porosity on the limit load and localization maps is also carried out. Finally, we conclude with some general comments and perspectives for future work.

2. The non-linear homogenization model

This section briefly describes the application of the "second-order" nonlinear homogenization model (SOM) of Danas and Ponte Castañeda (2009a) for porous elasto-plastic materials subjected to triaxial loading conditions. We first define the stress triaxiality and Lode parameters, followed by microstructural variables describing the volume fraction, shape, distribution and orientation of the voids. Next, building on the work of Aravas and Ponte Castañeda (2004), we develop consistent constitutive relations for the elastic and plastic deformations of the porous medium, and provide evolution laws for the above-mentioned microstructural variables, as well as the strain hardening law for the matrix material. Finally, expressions for the hardening rate and the localization conditions are derived.

2.1. Triaxial loading conditions: Stress triaxiality and Lode parameter

This subsection discusses the loading conditions and the associated stress measures used to distinguish between hydrostatic loading and different shear stress states. We consider purely triaxial loading conditions with the principal stresses $\sigma_1 = \sigma_{11}, \sigma_2 = \sigma_{22}$ and $\sigma_3 = \sigma_{33}$ ($\sigma_{ij} = 0$ for $i \neq j$) being aligned with the laboratory frame axes, $\mathbf{e}^{(1)}, \mathbf{e}^{(2)}$ and $\mathbf{e}^{(3)}$, respectively. This allows for the definition of alternative stress measures that are more appropriate for dilatational plasticity of porous materials. The three alternative measures are the hydrostatic (or mean) stress, σ_m, the von Mises equivalent (or effective) stress, σ_e, and the third invariant of the stress deviator, J_3, defined as

$$\sigma_m = \sigma_{kk}/3, \quad \sigma_e = \sqrt{3J_2} = \sqrt{3s_{ij}s_{ij}/2}, \quad J_3 = \det(s_{ij}), \tag{1}$$

where $s_{ij} = \sigma_{ij} - \sigma_m\delta_{ij}$ is the stress deviator. Using these definitions, we can readily define the stress triaxiality, X_Σ, and Lode angle, θ, or Lode parameter,[1] L, via the following expressions

$$X_\Sigma = \frac{\sigma_m}{\sigma_e}, \quad L = -\cos 3\theta = -\frac{27}{2}\frac{J_3}{\sigma_e^3}. \tag{2}$$

By definition, the range of values for the X_Σ and L, (or θ) are

$$-\infty < X_\Sigma < \infty, \quad \text{and} \quad -1 \leqslant L \leqslant 1 \quad \text{or} \quad 0 \leqslant \theta \leqslant \pi/3. \tag{3}$$

Then, relations (2) can be used to express the principal stresses as functions of X_Σ, σ_e and θ, such that

---

[1] Note that our choice for the Lode parameter L differs from the standard definition, $\mu = (2\sigma_1 - \sigma_3 - \sigma_2)/(\sigma_3 - \sigma_2)$, but the two parameters are simply related by $L = \mu(9 - \mu^2)/\sqrt{(\mu^2 + 3)^3}$, and therefore agree for the values −1, 0, and +1.

$$\frac{3}{2\sigma_e}\{\sigma_1, \sigma_2, \sigma_3\} = \left\{-\cos\left(\theta + \frac{\pi}{3}\right), -\cos\left(\theta - \frac{\pi}{3}\right), \cos\theta\right\} + \frac{3}{2}X_\Sigma\{1, 1, 1\}. \tag{4}$$

Fig. 2 shows the normalized principal stresses defined in (4) as a function of the Lode parameter L and Lode angle θ for (a) $X_\Sigma = 0$ and (b) $X_\Sigma = 1$. It is clear from Fig. 2(a) that for $L = -1$ or $\theta = 0$, the stress state is axisymmetric with one positive and two negative stresses (axisymmetric tension). On the other end, when $L = 1$ or $\theta = \pi/3$, the stress state is also axisymmetric but with two positive and one negative stresses (biaxial tension with axisymmetric compression). Note that these two different axisymmetric states lead to different evolution of the underlying microstructure and therefore to different overall responses as the deformation progresses. When, $L = 0$ or $\theta = \pi/6$, the stress state is in-plane shear with one stress identically equal to zero (e.g. plane stress state). The rest of the states are between axisymmetric and in-plane shear states. It should be noted that when the stress triaxiality is nonzero then the principal stresses are simply translated by a constant either upwards for $X_\Sigma > 0$, as shown in Fig. 2(b) for $X_\Sigma = 1$, or downwards for $X_\Sigma < 0$ (not shown here for brevity). Note also that $|X_\Sigma| \to \infty$ and $X_\Sigma = 0$ correspond to purely hydrostatic and purely deviatoric loadings, respectively.
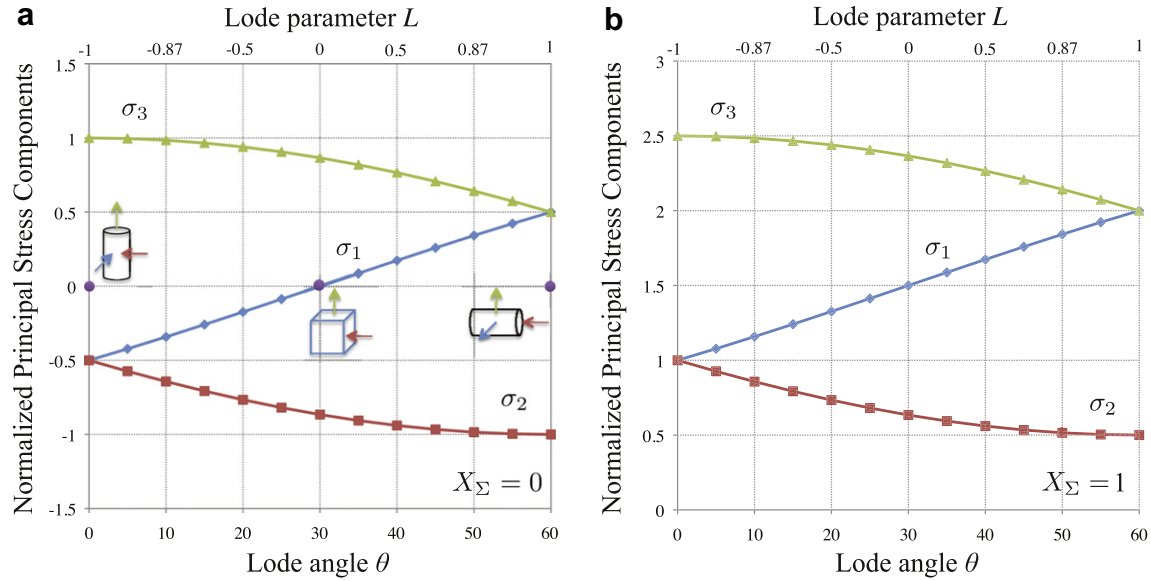
2.2. Microstructure

The porous material is composed of two phases. The matrix phase is elasto-plastic and isotropic following a J_2-flow rule with isotropic strain hardening described by the yield stress σ_y as a function of the accumulated equivalent plastic strain ε_M^p. The inclusion phase is vacuous and consists of initially spherical voids distributed uniformly and isotropically, such that the initial response of the porous medium is also isotropic. However, due to the finite deformations considered in this problem the voids evolve into non-spherical shapes and hence the porous medium becomes locally anisotropic (i.e., develops morphological anisotropy). Consequently, it is necessary to define microstructural variables that not only describe the volume fraction of the voids, as is the case in the models of Gurson (1977) and Nahshon and Hutchinson (2008), but also their shape, distribution and orientation.
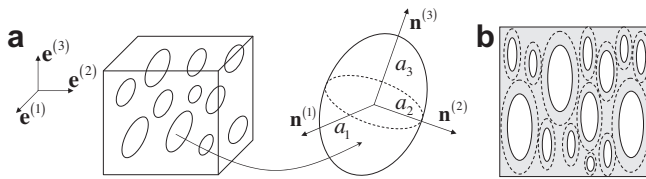
According to the schematic representation shown in Fig. 3(a) and at some finite deformation state, we consider that the porous material is characterized by a "particulate" microstructure consisting of ellipsoidal voids (i.e., with semi-axes $a_1 \neq a_2 \neq a_3$) aligned in a certain direction as a result of the previously described triaxial loading conditions. In addition, it is assumed (Willis, 1978; Ponte Castañeda and Willis, 1995) that the centers of the voids are distributed with ellipsoidal symmetry (see Fig. 3(b)). This description of a particulate microstructure represents a generalization of the Eshelby (1957) dilute microstructure to the non-dilute regime. In this work, which is based on the model of Danas and Ponte Castañeda (2009a), we will make the simplifying assumption that the ellipsoidal shape and orientation of the distribution function is identical to the ellipsoidal shape and orientation of the voids at each stage of the deformation. This is schematically shown in Fig. 3(b), where the dashed ellipsoids representing the pore distribution are taken to have the same ellipsoidal shape as the actual pores (in white). This assumption has been shown (Danas and Ponte Castañeda, 2009b) to provide accurate estimates, especially at small to moderate porosities. Nonetheless, it should be mentioned that, in general, the void distribution shape could be different from the void shape, as discussed by Ponte Castañeda and Willis (1995), and this effect can be accounted for at least approximately (Kailasam et al., 1997a).

Moreover, in the present study we consider purely triaxial loading conditions and initially isotropic materials (i.e., comprising

Fig. 2. Normalized principal stresses $\frac{3}{2\sigma_e}\{\sigma_1, \sigma_2, \sigma_3\}$, as a function of the Lode angle θ or equivalently the Lode parameter L. Parts (a) and (b) correspond to stress triaxialities $X_\Sigma = 0$ and $X_\Sigma = 1$, respectively.

Fig. 3. Graphical representation of the microstructure. Part (a) shows the local orientation axes $\mathbf{n}^{(i)}$ with $i = 1, 2, 3$ of a representative ellipsoidal void with semi-axis a_1, a_2 and a_3. Part (b) shows the a cross-section of the specimen where the "white" ellipsoids denote voids with ellipsoidal shape while the dashed ellipsoids refer to the distribution of their centers.

initially spherical voids). This implies that the orientation of the voids remains fixed and aligned with the triaxial loading conditions. Thus, the vectors $\mathbf{n}^{(i)}$ (with $i = 1, 2, 3$) denoting the orientation of the principal axes of the voids (see Fig. 3(a)) remain aligned with the principal laboratory axes $\mathbf{e}^{(i)}$. Consequently, the porous medium becomes, at most, orthotropic with finite deformations, with the axes of orthotropy coinciding with the principal axes of the ellipsoidal voids and the laboratory frame axes, i.e., with $\mathbf{n}^{(i)} = \mathbf{e}^{(i)}$. It should be emphasized, however, that the model of Danas and Ponte Castañeda (2009a) can account for more general loading conditions, non-spherical initial void shapes and rotation of voids, as has already been shown in Danas (2008) and Danas and Ponte Castañeda (2009b), but such a study is not carried out here because it will not be needed to describe the effects of interest in this work.

In view of the above hypotheses, the relevant internal variables describing the state of the microstructure in this problem are:

$$s_\alpha = \{\varepsilon_M^p, f, w_1, w_2\}, \tag{5}$$

where ε_M^p is the accumulated plastic strain in the undamaged matrix phase, f is the porosity (i.e., volume fraction of the voids), and $w_1 = a_3/a_1$ and $w_2 = a_3/a_2$ are two aspect ratios characterizing the ellipsoidal shape of the voids (with a_1, a_2 and a_3 denoting the principal semi-axes of the ellipsoidal voids) and their distribution function.

2.3. Elasto-plastic constitutive relations

The overall strain-rate $\boldsymbol{D}$ in the porous material is decomposed into its elastic and plastic parts via

$$\boldsymbol{D} = \boldsymbol{D}^e + \boldsymbol{D}^p, \tag{6}$$

where $\boldsymbol{D}^e$ and $\boldsymbol{D}^p$, respectively, denote the elastic and plastic parts. Note that due to the presence of voids the overall material behavior is compressible (i.e., pressure dependent) implying that the plastic strain-rate tensor is not deviatoric (i.e., $\boldsymbol{D}_{kk}^p \neq 0$). On the other hand, due to the triaxial loading conditions and the fact that the voids do not rotate during the deformation process, the overall spin as well as the microstructural spins are identically zero. In addition, in view of the fact that the pores can carry no loads and following Aravas and Ponte Castañeda (2004), it is assumed that the elastic and plastic parts of the strain rate can be estimated by independent, but consistent homogenization analyses.

Thus, the elastic response of the porous material is described in terms of an effective compliance tensor $\mathbf{M}$ via

$$D_{kl}^e = M_{ijkl}\dot{\sigma}_{ij}, \quad \text{with} \quad M_{ijkl} = M_{ijkl}^M + \frac{f}{1-f}Q_{ijkl}^{-1}, \tag{7}$$

where $\dot{\sigma}$ represents the material time derivative of the stress, which will be taken here to be given by the (partial) derivative with respect to time, since the stress is assumed to be uniform and the spin is zero, and $\mathbf{Q} = \mathbf{Q}(w_1, w_2, \mathbf{n}^{(i)} = \mathbf{e}^{(i)})$ is directly related to the well-known Hill or Eshelby tensor for ellipsoidal microstructures and its evaluation is detailed in Willis (1981) (see also Danas (2008)). The fourth-order tensor $\mathbf{M}^M$ is the compliance modulus of the matrix (metallic) phase and is taken to be isotropic such that

$$M_{ijkl}^M = \frac{1+v}{E}\left[\frac{1}{2}(\delta_{ik}\delta_{jl} + \delta_{il}\delta_{jk}) - \frac{v}{1+v}\delta_{ij}\delta_{kl}\right], \tag{8}$$

where E and v denote the elastic modulus and Poisson ratio, respectively.

On the other hand, the yield condition for the porous material can be written in the functional form

$$\Phi(\boldsymbol{\sigma}; s_\alpha) = \hat{\sigma}_{eq}(\boldsymbol{\sigma}; f, w_1, w_2) - \sigma_y(\varepsilon_M^p) = 0, \tag{9}$$

where $\hat{\sigma}_{eq}$ is a scalar function of the stress tensor and the microstructural variables, which is detailed in Danas and Ponte Castañeda (2009a) (c.f. Eqs. (25) and (28)), while σ_y is the effective stress governing flow of the undamaged matrix material and in general depends on the accumulated plastic strain ε_M^p in the matrix phase.

The overall plastic strain rate $\mathbf{D}^p$ of the porous material is then obtained from the normality rule via

$$D_{ij}^p = \dot{\Lambda} N_{ij}, \qquad N_{ij} = \frac{\partial \Phi}{\partial \sigma_{ij}}, \tag{10}$$

where $\dot{\Lambda} \geqslant 0$ is the plastic multiplier, which is determined by the consistency condition as discussed in subSection 2.5, and N_{ij} is the normal to the yield surface Φ. The reader is referred to Danas and Ponte Castañeda (2009a) for more detailed expressions for Φ and N_{ij}.

2.4. Evolution equations

Following the work of Ponte Castañeda and Zaidman (1994), Kailasam and Ponte Castañeda (1998), Aravas and Ponte Castañeda (2004) and Danas and Ponte Castañeda (2009a), evolution equations are given in this section for the microstructural variables ε_M^p, f, w_1 and w_2 defined in relation (5). Once again, in this work the orientation vectors remain aligned with the principal loading directions, i.e., $\mathbf{n}^{(i)} = \mathbf{e}^{(i)}$ ($i = 1, 2, 3$), during the deformation process.

The evolution equation for the accumulated plastic strain in the matrix phase ε_M^p is determined by the condition (Gurson, 1977) that the macroscopic plastic work $\sigma_{ij} D_{ij}^p$ be equal to the corresponding microscopic plastic work $(1 - f)\sigma_y \dot{\varepsilon}_M^p$, which implies that

$$\dot{\varepsilon}_M^p = \frac{\sigma_{ij} D_{ij}^p}{(1 - f)\sigma_y} = \dot{\Lambda} \frac{\sigma_{ij} N_{ij}}{(1 - f)\sigma_y}. \tag{11}$$

For strain hardening materials, σ_y is a function of ε_M^p, which, in general, is to be extracted from experimental uniaxial stress–strain curves. In our work, a rather general strain hardening law for $\sigma_y(\varepsilon_M^p)$ will be given in the results section.

Any changes of the pores are assumed to be only the result of plastic deformations (Aravas and Ponte Castañeda, 2004) while elastic deformations are considered to have a negligible effect on the evolution of the voids volume fraction. Noting further that the matrix material is plastically incompressible (J_2 plasticity), the evolution equation for the porosity f follows easily from the continuity equation and reads

$$\dot{f} = (1 - f) D_{kk}^p = \dot{\Lambda}(1 - f)\frac{\partial \Phi}{\partial \sigma_{kk}}. \tag{12}$$

We point out that void nucleation is not considered in the above relation but can be readily included by proper modification of (12) (e.g., Needleman and Rice (1978); Chu and Needleman (1980); Tvergaard (1990)).

The evolution of the aspect ratios w_1 and w_2, describing the shape of the voids, is given in terms of the average strain-rate in the vacuous phase $\mathbf{D}^v$ such that

$$\dot{w}_s = w_s(n_i^{(3)} n_j^{(3)} - n_i^{(s)} n_j^{(s)}) D_{ij}^v = \dot{\Lambda} y_w^{(s)}(\boldsymbol{\sigma}/\sigma_y; s_\alpha), \quad \text{with} \quad \mathbf{n}^{(i)} = \mathbf{e}^{(i)}, \tag{13}$$

and no sum on s = 1, 2. The average strain-rate $\mathbf{D}^v$ in the vacuous phase is estimated via the linear comparison material, as discussed in Danas and Ponte Castañeda (2009a) (see Eq. (76) in that reference). Finally, the associated functions $y_w^{(s)}$ have also been given in Danas and Ponte Castañeda (2009a) (see relation (80) in that reference) and will not be repeated here.

2.5. The consistency condition and the hardening rate

In this subsection, we determine the plastic multiplier $\dot{\Lambda}$ and hardening rate H by means of the consistency condition (Dafalias, 1985) for continuously applied loading, which in this case reads

$$\dot{\Phi} = \frac{\partial \Phi}{\partial \sigma_{kl}} \dot{\sigma}_{kl} + \frac{\partial \Phi}{\partial \varepsilon_M^p} \dot{\varepsilon}_M^p + \frac{\partial \Phi}{\partial f} \dot{f} + \sum_{s=1,2} \frac{\partial \Phi}{\partial w_s} \dot{w}_s = 0. \tag{14}$$

Substitution of the evolution Eqs. (11)–(13), and of $\partial \Phi / \partial \varepsilon_M^p = -d\sigma_y/d\varepsilon_M^p$, in this last relation provides the following expression for the plastic multiplier

$$\dot{\Lambda} = \frac{1}{H} \frac{\partial \Phi}{\partial \sigma_{kl}} \dot{\sigma}_{kl} = \frac{1}{H} N_{kl} \dot{\sigma}_{kl}, \tag{15}$$

where H is the hardening rate defined by

$$H = \frac{\sigma_{ij} N_{ij}}{(1 - f)\sigma_y} \frac{d\sigma_y}{d\varepsilon_M^p} - (1 - f)N_{kk}\frac{\partial \Phi}{\partial f} - \sum_{s=1,2} \frac{\partial \Phi}{\partial w_s} y_w^{(s)}. \tag{16}$$

The hardening rate is a measure of the overall hardening of the porous material. When $H > 0$, the material is said to harden, while when $H < 0$, it is said to soften. The critical point when $H = 0$ usually provides the transition from the hardening regime to the softening regime, and can be identified with the maximum stress or limit load of the material. Clearly, the maximum stress is important for stress-controlled boundary conditions, since the material will not be able to support stresses exceeding the limit load, and the material will fail at this point under increasing stress.

By observation of relation (16), we note that the first two terms of the right-hand side appear also in the Gurson (1977) and the Nahshon and Hutchinson (2008) models, and incorporate the effects of the matrix strain hardening and the evolving porosity (or damage in Nahshon and Hutchinson (2008)) on the overall response of the porous material. By contrast, in the present model, additional terms appear in (16), due to void shape changes. This last term of the right hand side in (16), which comprises the evolution of the two aspect ratios w_1 and w_2, affects the overall hardening rate of the porous material in a nontrivial manner. All these effects will be investigated in detail in the next section.

2.6. Localization conditions

In this subsection, we summarize the localization conditions corresponding to the loss of ellipticity of the governing equations and leading to non-unique solutions, bifurcations and instabilities, as described by Rice (1976). By making use of definition (15), the incremental constitutive relations (6), (7) and (10) describing the overall elasto-plastic response of the porous material can be written in the form

$$\dot{\sigma}_{ij} = L_{ijkl}^{inc} D_{kl}, \quad \text{where} \quad L_{ijkl}^{inc} = L_{ijkl} - \frac{N_{pq}L_{pqij}L_{klmn}N_{mn}}{H + N_{rs}L_{rsuv}N_{uv}} \tag{17}$$

is the effective incremental elasto-plastic modulus of the porous material, and $\mathbf{L} = \mathbf{M}^{-1}$ is the effective elastic modulus of the porous material.

Following Rice (1976), we consider an infinite porous medium with no initial imperfections, which implies that the trivial solution to this problem is homogenous deformation throughout the infinite region. Then, we look for conditions under which the deformation would localize inside a thin band leading to unloading outside the band, as shown schematically in Fig. 4. This second solution to the problem is a discontinuous bifurcation of the uniform solution and leads to a lower energy state than the uniform one. As already known, the specimen would tend to localize earlier if an initial imperfection were considered. However, the goal of the present study is to investigate pure material instabilities leaving aside any geometrical imperfections for a future study where actual boundary value problems resulting from experimental geometries will be investigated.

In any event, the condition for the localization of deformation inside a thin band with normal n_i becomes (Rice, 1976; Needleman and Rice, 1978)
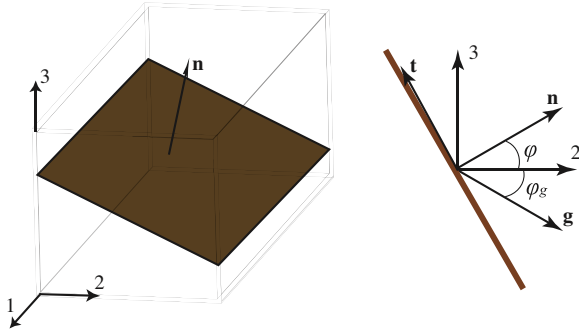
Fig. 4. Graphical representation of a localization band. The figure on the right shows the local system of coordinates, where **n** is the normal to the band and **t** is the tangent. The angle between **n** and **g** provides the deformation inside the band. For instance, if **n** $\perp$ **g**, the deformations inside the band is a simple shear. However, due to the compressibility of the porous material **g** is not, in general, perpendicular to **n** and the deformation inside the band can also have normal components (e.g. $n_i D_{ij} n_j \neq 0$), leading to the formation of a dilatant shear band.

$$\det \left[n_i L_{ijkl}^{inc} n_l + A_{jk} \right] = 0, \quad \text{where}$$

$$2A_{jk} = -\sigma_{jk} + \sigma_{js} n_s n_k + (n_p \sigma_{pq} n_q) \delta_{jk} - n_j n_r \sigma_{rk}. \tag{18}$$

When this localization condition is first met in a program of deformation, the difference between the total strain-rate inside and outside the band can be written as $\Delta D_{ij} = (g_i n_j + n_i g_j)/2$, with g_i being a function only of distance across the localization band $n_i x_i$ (with x_i being the position vector). The use of n_i and g_i provide information about the deformation state inside the localization band. For instance, in the case that the material is fully incompressible, it can be shown that g_i is perpendicular to n_i and parallel to the band tangent vector t_i which implies that the deformation state in the band is simple shear, i.e., a shear localization band. In the present study, however, the material is compressible due to the finite porosity, and can accommodate deformation states other than simple shear inside the band. In that case, n_i and g_i are not necessarily perpendicular to each other as shown in Fig. 4, which can lead to a nonzero normal component of the deformation state inside the band, i.e., $n_i \Delta D_{ij} n_j \neq 0$.

In connection with the above-described localization conditions, it should be emphasized that the (uniform) solutions obtained directly from the constitutive model for the porous material would cease to be valid at the point of the instability. Then, a post-bifurcation analysis would be required beyond this point. Such an analysis should make use of geometrical effects or initial imperfections and is outside the scope of the present work, which focuses on uniform solutions under fixed stress triaxialities and Lode parameter loadings throughout the entire deformation history. However, in the results to be described in the next section, the (uniform) solutions will still be shown beyond the onset of said instabilities, mostly because they are suggestive of the mode of the onset of the instability. Of course, such solutions are not meant to be representative of what actually happens beyond the instability. As already known from investigation in other contexts (e.g., failure of fiber-reinforced composites), the final failure mode requires the full post-bifurcation analysis. More often than not, such failure modes are inherently different from the mode of the onset of the instability.

3. Results and discussion

As already mentioned in the previous section, our objective is to investigate the effects of the stress triaxiality X_Σ and Lode parameter L (or Lode angle θ) on the macroscopic response and failure of porous elasto-plastic materials subjected to triaxial loading conditions. Given the fact that a maximum stress is expected, in this

work the strain rate D_{33} will be prescribed, together with the values of X_Σ and L, which will serve to determine all three (principal) stresses, σ_1, σ_2 and σ_3, as well as the evolution of the microstructural variables, the porosity f, and the average aspect ratios, w_1 and w_2, as functions of time t. However, it will be convenient to use as a time-like variable the total equivalent strain $\varepsilon_e = \int_t \sqrt{2D_{ij}' D_{ij}'/3} dt$, with D_{ij}' denoting the strain-rate deviator, and to consider the overall von Mises equivalent stress σ_e instead of the individual stress components in the characterization of the macroscopic response. Because of the special loading conditions imposed, it can be shown that the maximum on the σ_e versus ε_e plots will correspond exactly to a vanishing hardening rate $H = 0$, indicating a possible instability under stress-controlled loading conditions. In addition, the loss of ellipticity condition will be determined for the material making use of the condition (18). For completeness, a comparison will also be made between the predictions of the "second-order" model (SOM) of Danas and Ponte Castañeda (2009a) and the modified Gurson model (MGUR) proposed by Nahshon and Hutchinson (2008). In keeping with standard practice (Barsoum and Faleskog, 2007a), the maximum stress (i.e., the locus of points where $H = 0$) and loss of ellipticity (LOE) conditions will be displayed in terms of the total equivalent plastic strain (or effective plastic strain) $\varepsilon_e^p = \int_t \sqrt{2(D_{ij}^p)'(D_{ij}^p)'/3} dt$, with $(D_{ij}^p)'$ denoting the plastic strain-rate deviator. In this work, the resistance of the material to failure by either condition will be referred to as the overall ductility. Furthermore, it should be emphasized, that as a consequence of the very small magnitude of the overall elastic strains, the difference between the overall total strain and the overall plastic strain is very small for all practical purposes. Finally, a parametric study will be carried out to investigate the influence of different matrix strain hardening exponents and initial porosities on the limit load and LOE maps.

3.1. Material parameters and initial conditions

The Young's modulus and Poisson's ratio of the matrix phase are taken to be $E = 200$ GPa and $v = 0.3$, respectively, and the matrix phase to exhibit isotropic strain hardening following the law[2]

$$\sigma_y(\varepsilon_M^p) = \sigma_0 \left(1 + \frac{\varepsilon_M^p}{\varepsilon_0} \right)^N, \qquad \varepsilon_0 = \sigma_0/E. \tag{19}$$

In this expression, σ_0 and ε_0 denote the initial yield stress and yield strain of the matrix material (i.e., the material with $f = 0$), and $N \leqslant 1$ is the strain hardening exponent. Typical values for these parameters are $\sigma_0 = 200$ MPa and $N = 0.1$, which will be used throughout this work except in Section 3.4 where a parametric study is carried out with $N = 0.01, 0.05, 0.1$ and 0.2.

The matrix phase is taken to be initially unloaded with zero accumulated plastic strain $\varepsilon_M^p = 0$, while the voids are initially spherical with $w_1 = w_2 = 1$. The initial porosity is taken to be $f_0 = 1\%$ except in Section 3.4 where a parametric study is carried out with $f_0 = 0.1\%, 1\%$ and 5%. It should be noted that the dependence of the failure maps on the Young's modulus, and Poisson's ratio has been found to be weak, and for this reason no results will be reported here for different values of these parameters.

3.2. Stress–strain response and microstructure evolution results

In order to investigate the main effects of the stress triaxiality and Lode parameter on the effective response of the porous

---
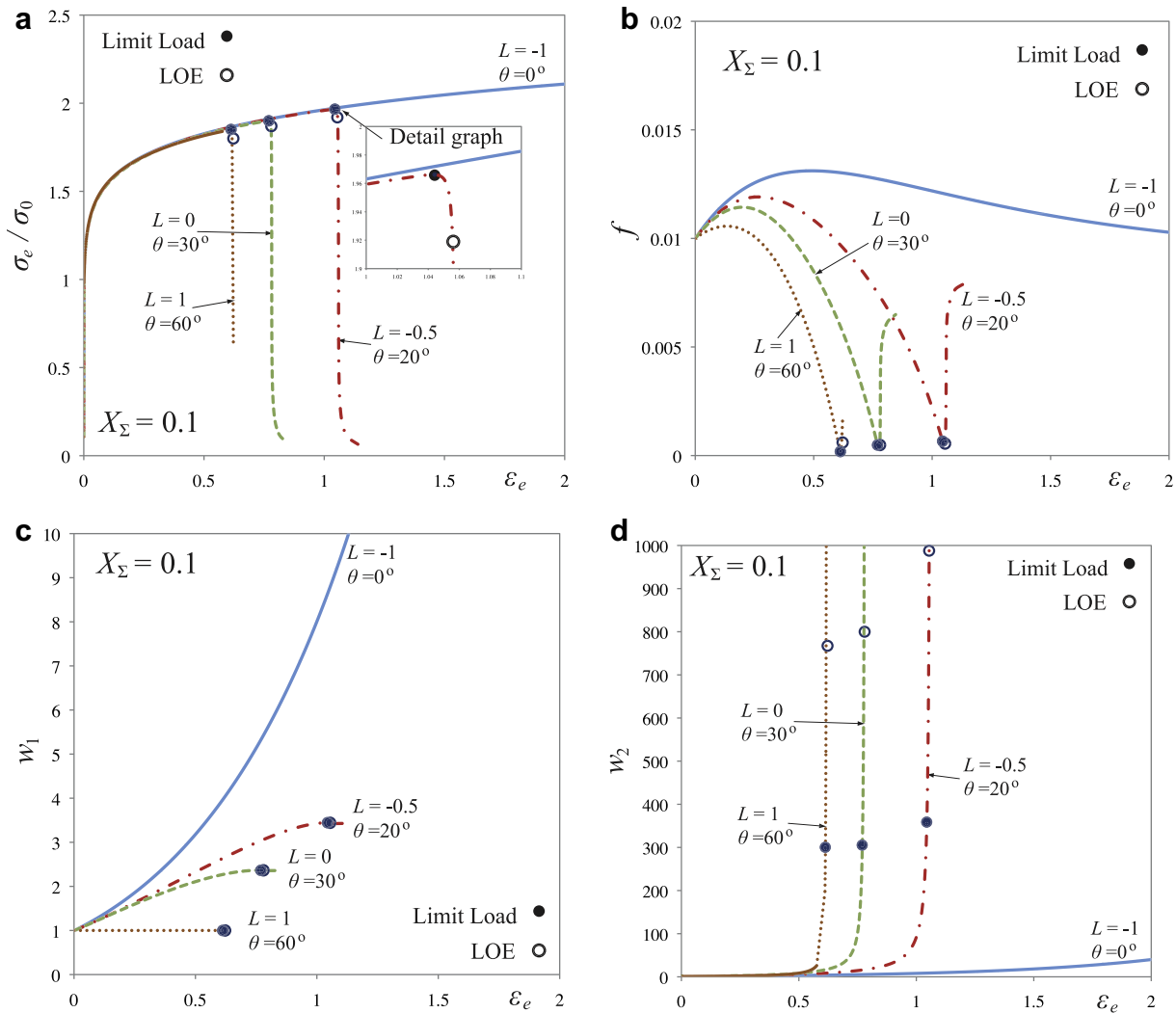
Fig. 5. Plots of the SOM estimates for (a) the equivalent stress σ_e, (b) the porosity f, and the aspect ratios (c) w_1 and (d) w_2 as a function of the equivalent strain ε_e, for a low value of the stress triaxiality ($X_\Sigma = 0.1$) and four values of the Lode parameter. The influence of the Lode parameter is dramatic at low triaxialities mainly due to the extremely sharp evolution of the aspect ratio w_2 in (d). The strain hardening exponent is $N = 0.1$ and the initial porosity $f_0 = 1\%$. The inset in part (a) shows a blow up of the region around the maximum stress for $L = -0.5$ (or $\theta = 20^o$).

material, we show results for three representative values of stress triaxialities, $X_\Sigma = 0.1, 0.6, 1$, and four of the Lode parameter, L=−1,−0.5,0,1 (or Lode angle $\theta = 0, 20, 30, 60^o$, respectively).

Fig. 5 shows plots of (a) the equivalent stress σ_e, (b) the porosity f, and the aspect ratios (c) w_1 and (d) w_2, as a function of the equivalent strain ε_e, for given values of the Lode parameter and a *low* value of the stress triaxiality ($X_\Sigma = 0.1$). The main observation in Fig. 5a is that the Lode parameter strongly affects the onset of softening (i.e., maximum load) and localization of the porous material. For axisymmetric tensile loadings ($L = -1$), the stress increases following the prescribed strain hardening law of the matrix phase ($N = 0.1$ here). On the other hand, for $L = -0.5, 0,$ and 1, we observe abrupt drops in σ_e at different levels of the total strain ε_e, indicating a sudden loss in the load-carrying capacity of the material. In addition, after the maximum stress σ_e (see inset graph in Fig. 5(a) or limit load (black dot on the graph) strong softening of the material is observed eventually leading to localization and hence loss of ellipticity (open circle on the graph) of the homogenized equations.

With the objective of shedding light on the mechanism leading to this sharp stress drop, it is necessary to consider the evolution of the microstructural variables, f, w_1 and w_2, provided in Figs. 5 (b),

(c) and (d), respectively. In part (b), we observe an overall reduction in the porosity f as a function of ε_e up to the point of the limit load (black dot on the graph), followed by a sharp increase in f shortly after the maximum stress has been achieved. It is clear by Fig. 5(b) that at the strain level at which the limit load and loss of ellipticity occur, the porosity is still very small. Therefore, the corresponding stress drop observed in part (a) cannot be due to the increase in the porosity, and the only microstructural variables that can possibly affect the overall response of the porous material are the aspect ratios, w_1 and w_2. As shown in part (c), w_1 can become rather large for $L = -1$, but remains below the value of 5 for $L > -0.5$. On the other hand, as shown in part (d), w_2 increases very fast for all values of $L > -1$. In particular, for $L = 1$ (corresponding to axisymmetric compression along the x_2 direction, see Fig. 2(a)), $w_1 = 1$, while w_2 blows up at a certain "critical" value of ε_e (around 0.6). This means that the voids *collapse* in the x_2 direction, becoming flattened cracks (lying in the $x_1 - x_3$ plane) with $a_2 \to 0$, while the material becomes locally anisotropic (i.e., exhibits strong morphological anisotropy due to the very significant void shape changes). However, since the porosity f remains finite at this "critical" point where $a_2 \to 0, a_1 = a_3$ must tend to infinity, suggesting coalescence of the voids in the $x_1 - x_3$ plane.
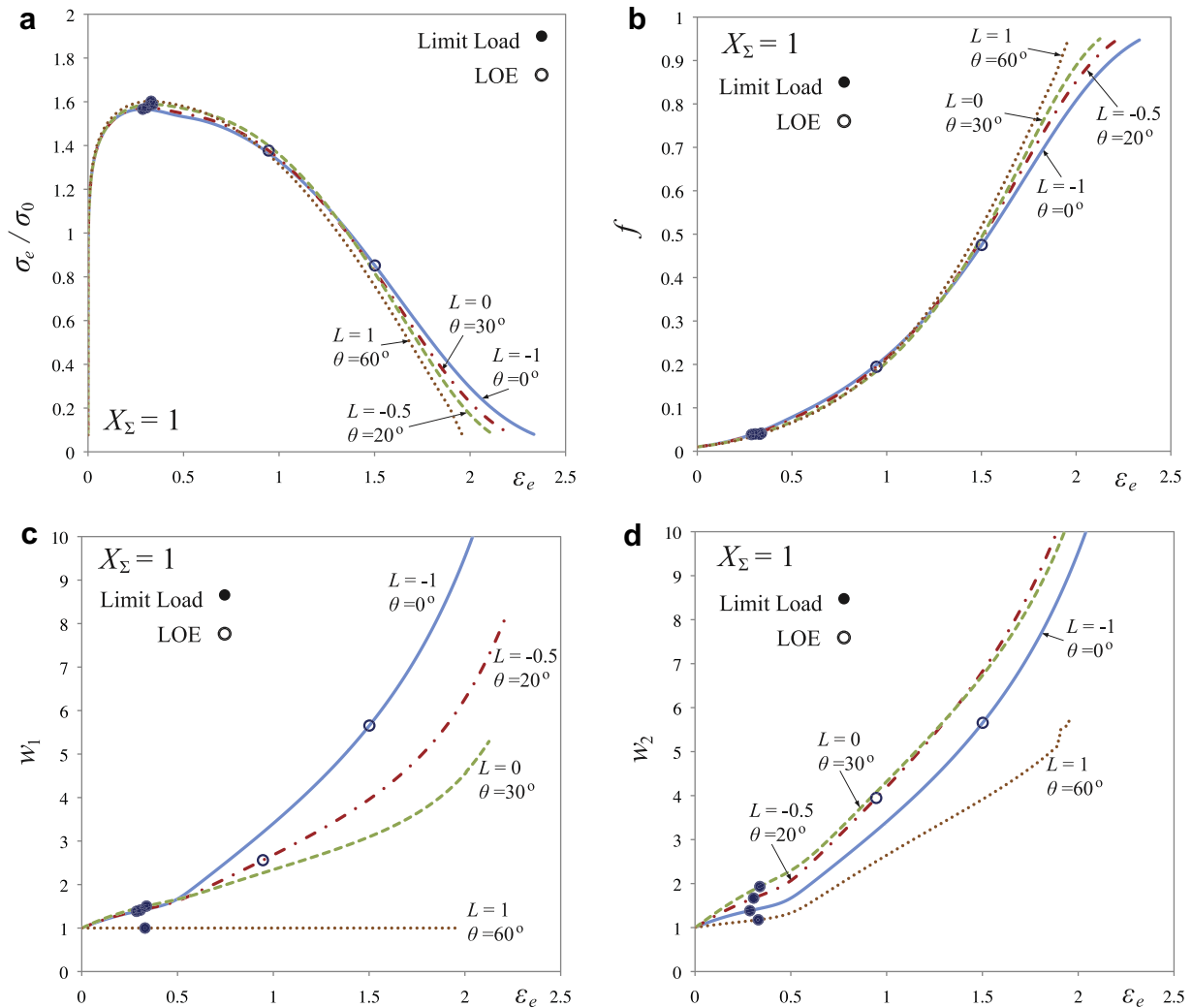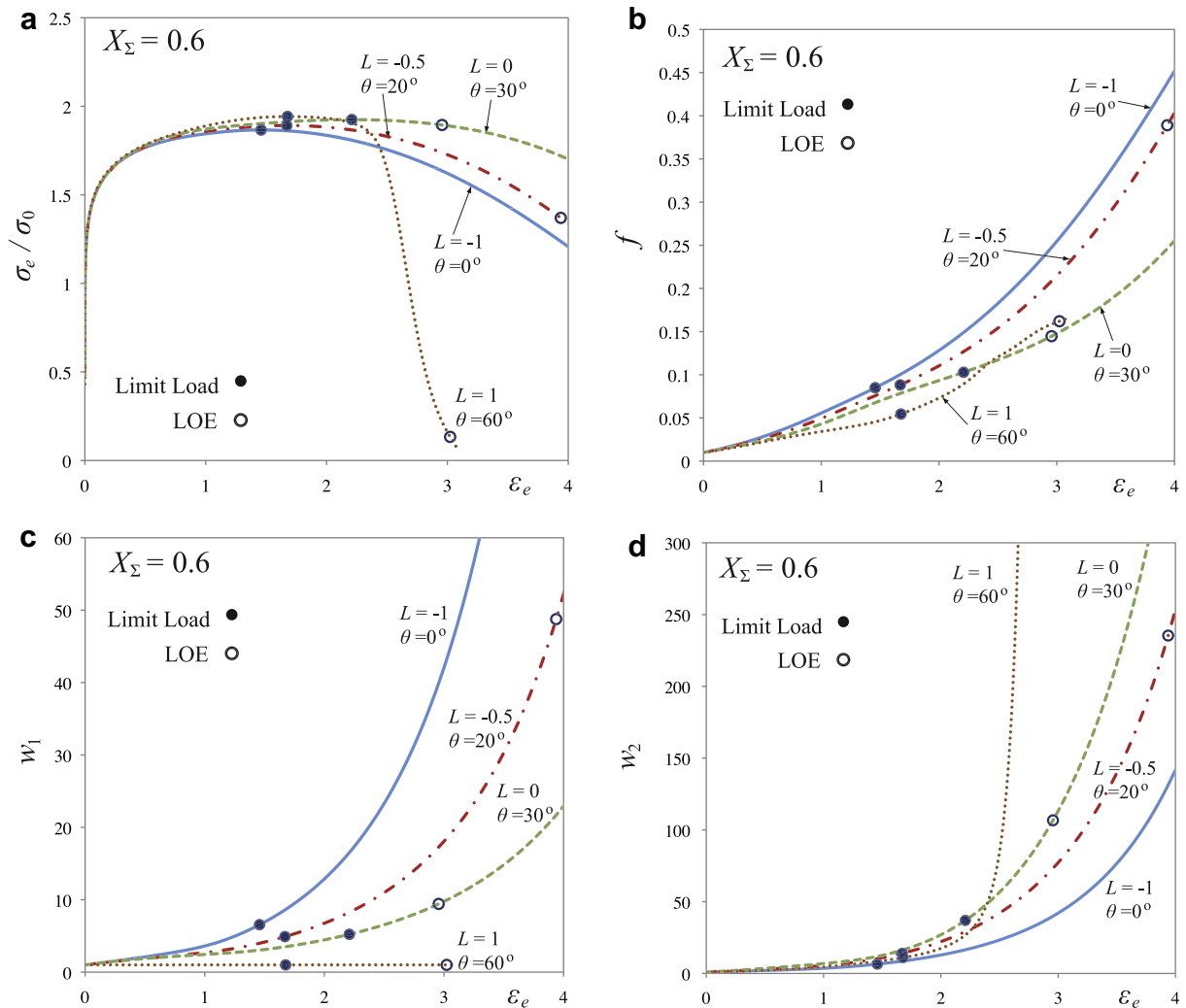
Fig. 6. Plots of the SOM estimates for (a) the equivalent stress σ_e, (b) the porosity f, and the aspect ratios (c) w_1 and (d) w_2 as a function of the equivalent strain ε_e, for a high value of the stress triaxiality ($X_\Sigma = 1$) and four values of the Lode parameter. The influence of the Lode parameter becomes negligible in this case since the response of the porous material is dominated by the significant evolution of porosity f. The strain hardening exponent is $N = 0.1$ and the initial porosity $f_0 = 1\%$.

To clarify this failure mechanism further, it is recalled here that the aspect ratios serve to denote both the shape of the voids as well as the shape of their distribution function. Hence, as $a_2 \to 0$ and $a_1 = a_3 \to \infty$ both the shape of the voids and the shape of their distribution function become extremely flat in the $x_1 - x_3$ plane. This observation together with the fact that the porosity is small but finite, implies that the pores grow without a bound in the $x_1 - x_3$ plane, eventually linking up to form "layers" of pores in the solid material, which can be associated with void coalescence in that plane and subsequent loss of the load-carrying capacity of the material in the transverse direction. Such a failure mechanism would be consistent with the "flat" dimples observed in Fig. 1(b) from the experimental results of Barsoum and Faleskog (2007a) at low stress triaxialities. (Note, however, that the presence of the second-phase particles may interfere with the collapse of the voids, and should be accounted for in situations where the voids are not pre-existing, but instead nucleate from second-phase particles.) For other values of L with $-1 < L < 1$, essentially the same mechanism is observed except that in this case the pores also change shape in the collapse plane ($x_1 - x_3$). However, as can be seen in Figs. 5a and d, the effect becomes more pronounced as the value of L increases from -1 toward $+1$. At the extreme value of $L = -1$, the shape of the pores is constrained to remain circular

in the $x_1 - x_2$ cross-section, and this kinematic restriction prevents collapse of the pores, explaining the lack of a maximum stress point and corresponding loss of ellipticity in this case.

Fig. 6 shows plots of σ_e, f, w_1 and w_2 as a function of the equivalent strain ε_e, for several fixed values of the Lode parameter L and for a *high* value of the stress triaxiality ($X_\Sigma = 1$). The main result is that the effect of the Lode parameter on the overall mechanical response of the porous material is negligible, as can be seen in Fig. 6(a), since all the $\sigma_e - \varepsilon_e$ curves almost coincide. In particular, they exhibit a limit load at rather low strains and then smooth but significant softening as the deformation progresses. Note further that for $L = 1$ no LOE (open circles on the plots) is detected. However, failure of the porous material is not excluded (see the significant drop of the material loading capacity). As already pointed out by Rice (1976), this type of localization analysis based on uniform fields only provides an upper bound for failure while the presence of more realistic geometries can lead to localization much earlier.

The fact that the stress–strain curve is independent of the Lode parameter at $X_\Sigma = 1$ is easily explained by referring to Fig. 6(b), where the increase of porosity is significant for all values of the Lode parameter ($L = -1, -0.5, 0, 1$). In addition, looking at parts (c) and, especially, (d), we note that the void shape still evolves as a function of ε_e, but in a much weaker manner than for the

Fig. 7. Plots of the SOM estimates for (a) the equivalent stress σ_e, (b) the porosity f, and the aspect ratios (c) w_1 and (d) w_2 as a function of the equivalent strain ε_e, for a moderate value of the stress triaxiality ($X_\Sigma = 0.6$) and four values of the Lode parameter. The influence of the Lode parameter is significant in this case of moderate triaxiality indicating a transition mechanism from void collapse-dominated response for $L = 1$ to porosity-dominated response for $L \leqslant 0$. The strain hardening exponent is $N = 0.1$ and the initial porosity $f_0 = 1\%$.

previous case of $X_\Sigma = 0.1$. This indicates that the main softening mechanism in this high-triaxiality situation ($X_\Sigma = 1$) is clearly the evolution of porosity which is found to lead to significant softening of the effective response of the porous material. Note that this void-growth mechanism is expected to eventually lead to (three-dimensional) coalescence of the voids, and failure consistent with the deep dimples observed in the micrographs shown in Fig. 1(d) from the experimental results of Barsoum and Faleskog (2007a). Also, it is clear that the dominance of the evolution of porosity will prevail at larger stress triaxialities $X_\Sigma > 1$ not shown here (but see Danas and Ponte Castañeda (2009b)).

Fig. 7 shows plots of σ_e, f, w_1 and w_2 as a function of the equivalent strain ε_e for several values of the Lode parameter ($L = -1, -0.5, 0, 1$) and a *moderate* value of the stress triaxiality ($X_\Sigma = 0.6$). As can be observed in part (a), for $L = -1, -0.5, 0$, the stress curves reach a maximum (limit load) and then smoothly decrease, leading to overall softening for larger values of the strain ε_e. On the other hand, the $L = 1$ curve exhibits a sharp decrease of σ_e, albeit less dramatic than the corresponding one for $X_\Sigma = 0.1$. Moreover, it is interesting to note that the limit load occurs at lower ε_e when $L = -1$ than when $L = -0.5$ or $L = 0$. In fact, as L increases to

the value of 0, the critical strain ε_e at which the limit load occurs increases, whereas it decreases again as we increase further L toward the value of 1. This non-monotonic dependence on the Lode parameter L can be understood by considering the evolution of the microstructure shown in parts (b), (c) and (d) of Fig. 7. In Fig. 7(b), the porosity increases for all values of L, with the weakest growth observed for $L = 1$ and the strongest for $L = -1$ (reaching relatively high values at this last case). In turn, in part (c), w_1 increases similarly to the previous case of $X_\Sigma = 0.1$. In Fig. 7(d), considering $L = -0.5, 0$, we find that w_2 does not exhibit the sharp increase observed in Fig. 5(d) for $X_\Sigma = 0.1$ (for the same values of L). This explains the smooth softening (gentle decrease of σ_e) of the porous material observed in the curves of part (a), for $L = -1, -0.5$, and 0. By contrast, when $L = 1$, w_2 increases sharply attaining very high values corresponding to void collapse, leading to a sharp drop of the stress (similar to the corresponding case for $X_\Sigma = 0.1$). This example reveals that at moderate values of the stress triaxiality (e.g., $X_\Sigma = 0.6$) there is a transition from softening induced by *void growth* for $L = -1, -0.5$ to failure induced by *void collapse* for $L = 1$, while for $L = 0$ the failure mechanism is a combination of both void shape and porosity effects.
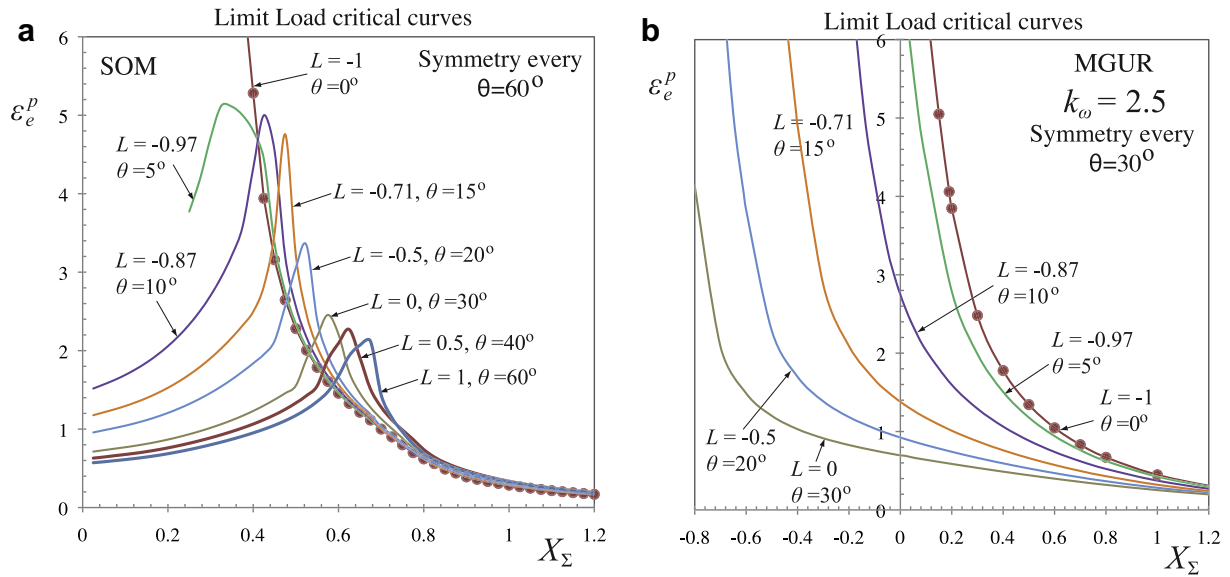
Fig. 8. Limit load failure curves as predicted by (a) the SOM model and (b) the MGUR model with $k_\omega = 2.5$, as a function of the stress triaxiality X_Σ and the Lode parameter L (or θ). The critical equivalent plastic strain ε_e^p at the limit load where the hardening rate $H = 0$ provides a "macroscopic" measure of the overall ductility of the material. The strain hardening exponent is $N = 0.1$ and the initial porosity $f_0 = 1\%$.
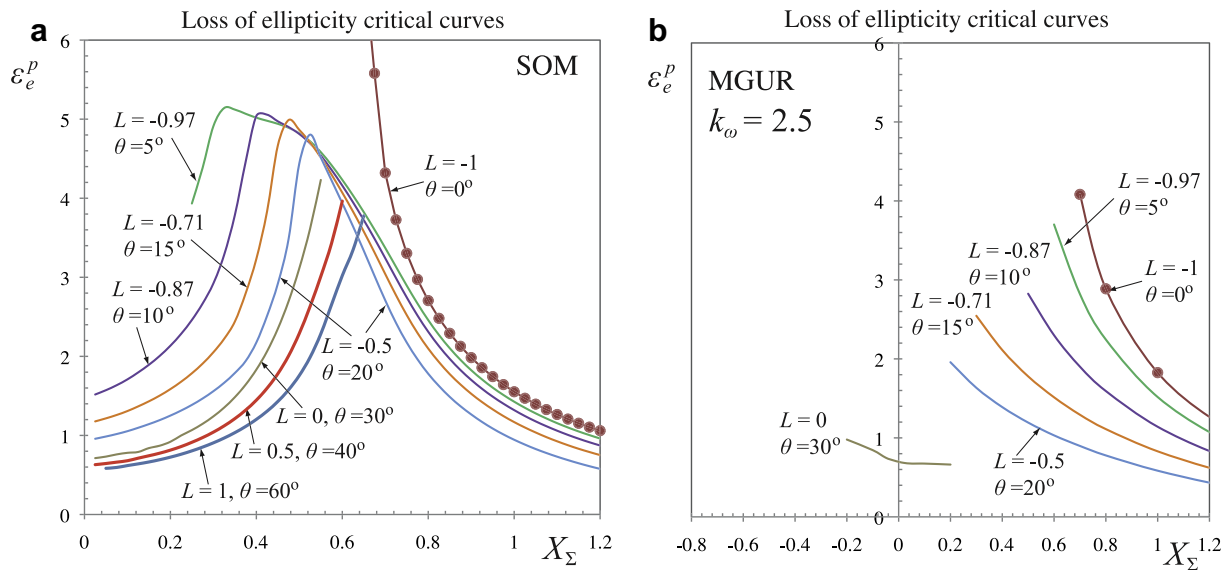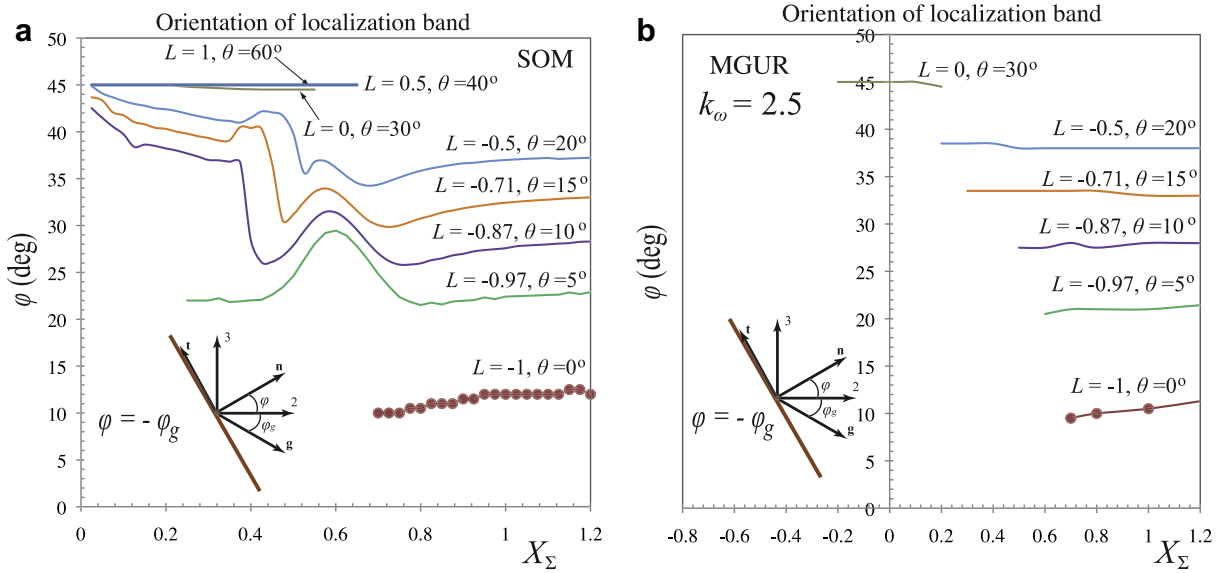

Fig. 9. Loss of ellipticity failure curves as predicted by (a) the SOM model and (b) the MGUR model with $k_\omega = 2.5$, as a function of the stress triaxiality X_Σ and the Lode parameter L (or θ). The critical equivalent plastic strain ε_e^p at loss of ellipticity, with localization of deformation into dilatant shear bands taking place, provides an alternative "macroscopic" measure of the overall ductility of the material. The strain hardening exponent is $N = 0.1$ and the initial porosity $f_0 = 1\%$.

## 3.3. Limit load and loss of ellipticity failure curves

The purpose of this section is to analyze and summarize the effect of the stress triaxiality and the Lode parameter on the limit load and LOE failure instabilities. For completeness, the predictions of the present "second-order" model (SOM) will be compared and contrasted with the corresponding predictions of the recently proposed phenomenological model of Nahshon and Hutchinson (2008), labeled here as MGUR, which is based on an empirical modification of the well-known Gurson (1977) model. The MGUR model requires the choice of the parameter k_ω (see expression (10) in the referenced publication for the definition of k_ω) which is directly related to the Lode parameter. For the identification of this parameter several experiments have been performed indicating a value of

k_ω between 1 and 3. In our study, we make the choice $k_\omega = 2.5$, without insisting on the quantitative aspects of the results, but rather on their qualitative nature.

Fig. 8 shows plots of the SOM and MGUR predictions for the critical equivalent plastic strain ε_e^p attained at the limit load (i.e., the maximum in the $\sigma_e - \varepsilon_e$ curve, or equivalently, the critical hardening rate $H = 0$), as a function of the stress triaxiality X_Σ, for fixed values of the Lode parameter L (or Lode angle θ). As depicted in Fig. 8(a), for fixed values of L, the SOM predictions clearly exhibit two regimes, a low-triaxiality regime where the material ductility increases with increasing triaxiality, followed by a second, high-triaxiality regime with the opposite trend. The two regimes are separated by a rather abrupt transition, or "high-ductility peak", and as already pointed out, in the low-triaxiality regime,

Fig. 10. Orientation of the localization band defined by the angle φ as predicted by (a) the SOM model and (b) the MGUR model with $k_\omega = 2.5$, as a function of the stress triaxiality X_Σ and the Lode parameter L (or θ). The strain hardening exponent is $N = 0.1$ and the initial porosity $f_0 = 1\%$.
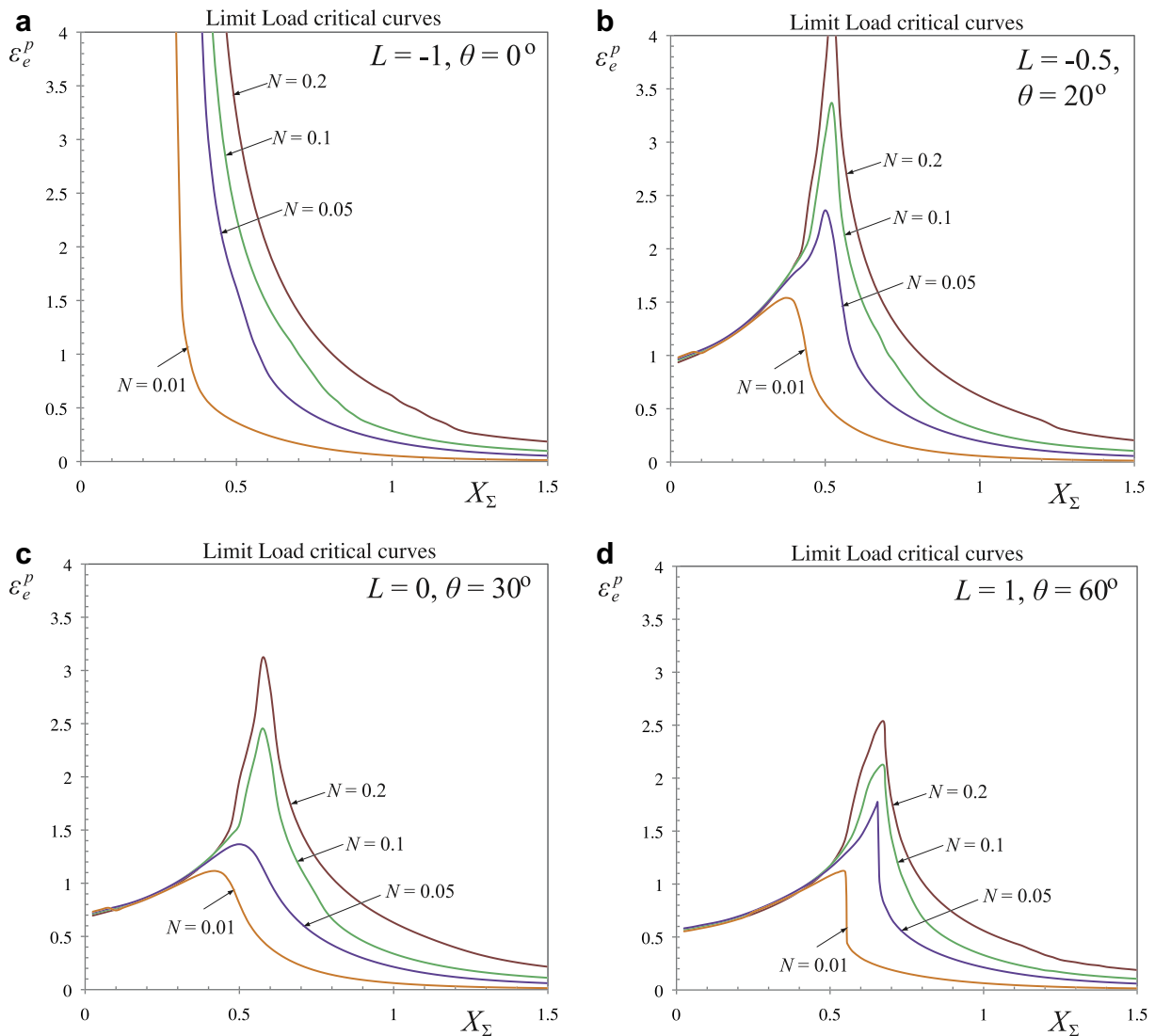
Fig. 11. SOM limit load failure curves as a function of the stress triaxiality X_Σ and the strain hardening exponent $N = 0.01, 0.05, 0.1, 0.2$ for various values of the Lode parameter: (a) $L = -1$, (b) $L = -0.5$, (c) $L = 0$ and (d) $L = 1$. The initial porosity $f_0 = 1\%$.

the source of the instability is void collapse, while in the second, it is void growth. In addition, the high-triaxiality regime is rather insensitive to the Lode parameter, while the low-triaxiality regime and the transition between the two is strongly dependent on the Lode parameter, with the ductility increasing from a value of $L = +1$ to the value of $L = -1$ (where no void collapse is possible and therefore no low-triaxiality regime is observed). In this connection, the predictions of the SOM model for failure at the limit load appear to be qualitatively consistent with the experimental results of Barsoum and Faleskog (2007a), presented in Fig. 1(a). Note, however, that in the results of Fig. 1(a), the stress triaxiality evolves (and is non-uniform) during the deformation process as a consequence of the complex geometry of the experimental setup, and, hence, comparisons of the SOM results (which involve uniform fields and fixed triaxiality) with the experimental results of Barsoum and Faleskog (2007a) can only be qualitative in nature.

By contrast, as shown in Fig. 8(b), the MGUR model predictions exhibit qualitatively different behavior for the limit load failure curves. As expected from the way in which it was constructed, the limit load curves depend strongly on the Lode parameter, but in a manner that is monotonic with respect to the triaxiality and therefore does not exhibit the two different regimes and particularly the high-ductility peaks predicted by the SOM model and shown by the experimental results in Fig. 1(a). This significant difference found between these two models is clearly linked to the fact that the SOM model can account for void shape changes and therefore can capture the void collapse mechanism contrary to the MGUR model which assumes spherical void shapes during the entire deformation process. In addition, the MGUR predictions for the limit load exhibit a symmetry of $\theta = 30^o$, implying in particular that the limit loads for $L = -1$ (corresponding to uniaxial tension) and $L = 1$ (biaxial tension with uniaxial compression) are identical. This result is a direct consequence of the ad-hoc quadratic character of the dependence of the MGUR model on the Lode parameter (see relation (4) in Nahshon and Hutchinson (2008)), and is in sharp contrast with the SOM model which, for low triaxiality, predicts low ductility for $L = 1$, but very high ductility for $L = -1$. It is also worth noting that the MGUR model predicts the existence of limit loads for negative values of the stress triaxialities. This is also in contrast with the the SOM model which predicts that the hardening produced by the porosity reduction with negative triaxialities completely overwhelms any softening due to changes in the shape of the voids, and therefore the material continues to harden all the way up to complete void closure.

Fig. 9 shows SOM and MGUR predictions for the critical equivalent plastic strain ε_e^p at localization of the deformation, or loss of ellipticity (LOE), defined by condition (18), as functions of the stress triaxiality X_Σ, for several values of the Lode parameter L (or Lode angle θ). As shown in Fig. 9(a), the SOM predictions for LOE are roughly similar to those for the limit load depicted in Fig. 8(a), and also exhibit two sharply separated regimes. However, in addition to the strong dependence in the Lode angle observed in the low-triaxiality regime, there is also some (smaller) sensitivity in the high-triaxiality regime with the ductility decreasing as the value of L is increased from -1. In fact, no LOE is detected for values of $L > 0$ and $X_\Sigma > 0.5 - 0.7$, but note that the stress drops to zero for sufficiently high deformation as a consequence of the continued porosity growth discussed in the previous section, while other well-known failure mechanisms such as high-triaxiality void coalescence are present (see review work of Benzerga and Leblond (2010)).

On the other hand, as shown in Fig. 9(b), the MGUR model predicts LOE only for values of $L \leqslant 0$, while no LOE is detected for $L > 0$ (for all stress triaxialities X_Σ). Furthermore, contrary to the corresponding SOM predictions, no LOE is detected for low triaxialities except for a small branch for $L = 0$. This is a direct consequence

of the fact that the MGUR model remains isotropic during the entire deformation process as a result of no void shape changes, and therefore completely misses the morphological anisotropy developed due to the significant void shape evolution in the low-triaxiality regime. Finally, it is noted in the context of this figure that for the special values of $L = 1$ and -1, the MGUR model reduces to the Gurson model and note that the predictions for LOE for these two values are different (in one case there is LOE and in the other there is not), which in view of the identical predictions for the limit load for these two cases demonstrates the sensitivity of the LOE condition to the pertinent kinematical conditions.

Finally, in Fig. 10, the earlier LOE results are completed by depicting the orientation of the localization band in terms of the angle φ that defines the orientation of the normal to the band $\mathbf{n}$ with respect to the x_2 axis (see inset sketches in the plots). The SOM and the MGUR results are shown in Fig. 10(a) and Fig. 10(b), respectively, as a function of the stress triaxiality X_Σ for several values of the Lode parameter L (or Lode angle θ). The complementary angle φ_g, associated with the vector $\mathbf{g}$, which controls the type of deformation inside the band, is found to be $\varphi_g = -\varphi$ for both the SOM and the MGUR models. Moreover, note that the normal to the band $\mathbf{n}$, as predicted by both the SOM and the MGUR models, lies on the $x_2 - x_3$ plane. In particular, for the case when $\varphi = -\varphi_g = 45^o$ (i.e., $\mathbf{n} \perp \mathbf{g}$), the state of deformation inside the band is a simple shear and thus formation of a shear localization band is produced. This is the case for $L \geqslant 0$ (or $\theta \geqslant 30^o$) for the SOM model and $L = 0$ (or $\theta = 30^o$) for the MGUR model. Note that, in accord with the earlier discussions, the MGUR model predicts no loss of ellipticity for $L > 0$ and hence no angles are shown for these cases. On the other hand, for $L < 0$, we observe for both the SOM and the MGUR models that the predicted localization band angle is smaller than 45° and hence the state of deformation inside the band is a combination of shear plus dilatation across the band (in the direction of the normal to the band). The lowest value for φ is attained in both models for $L = -1$, where the localization band is found to be at an angle of about 10°. It should be emphasized that at large triaxialities the SOM and the MGUR models predict very similar localization angles, highlighting once again the fact that the main difference between the models is for low triaxialities when changes in the shape of the pores become possible.
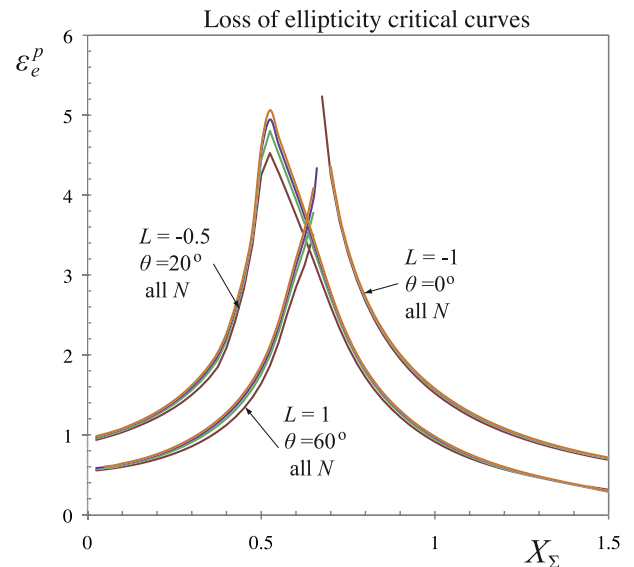

Fig. 12. SOM loss of ellipticity (LOE) failure curves as a function of the stress triaxiality X_Σ and the strain hardening exponent $N = 0.01, 0.05, 0.1, 0.2$ for various values of the Lode parameter: $L = -1, -0.5, 1$. The initial porosity $f_0 = 1\%$.

3.4. Influence of strain hardening exponent and initial porosity on failure curves

Making use of the SOM model, a parametric study is carried out to investigate the effect of the strain hardening exponent of the matrix phase and the initial porosity on the limit load and loss of ellipticity (LOE) failure curves. Thus, the following figures show plots of the critical equivalent plastic strain ε_e^p attained at the limit load (i.e., maximum in the $\sigma_e - \varepsilon_e$ curve, or equivalently critical hardening rate $H = 0$), and at loss of ellipticity (LOE), or localization of deformation (given by (18)), as functions of the stress triaxiality X_Σ and the Lode parameter L (or Lode angle θ).

Fig. 11 shows limit load maps for (a) $L = -1$, (b) $L = -0.5$, (c) $L = 0$ and (d) $L = 1$ as a function of the stress triaxiality X_Σ using different strain hardening exponents for the matrix phase, $N = 0.01, 0.05, 0.1, 0.2$. (Note that $N = 0$ and $N = 1$ correspond to ideally plastic and linear hardening behaviors. respectively.) The limit load failure curves are strongly dependent on N for moderate and high triaxialities such as $X_\Sigma > 0.4$, as observed in all parts of Fig. 11. By contrast, at low stress triaxialities ($X_\Sigma < 0.35$) and $L > -1$, i.e., Fig. 11(b), (c), (d), the limit load failure curves exhibit negligible dependence on the strain hardening exponent. This is

due to the fact that at low X_Σ, the limit load occurs in such an abrupt manner due to the very fast void shape changes (observed in the context of Fig. 5) that the hardening of the matrix plays almost no role on the overall softening mechanism of the porous material. On the other hand, as the triaxiality increases the growth of porosity dominates the limit load mechanism. The porosity growth however is rather smooth allowing the strain hardening exponent to play a dominant role on the overall softening of the material. In contrast, as shown in Fig. 12, the strain hardening exponent N has only a negligible effect on the LOE predictions. This suggests that once the material enters the softening regime, kinematics controls the localization mechanism and hence the effect of N is not important.

Fig. 13 shows the limit load failure curves as a function of the stress triaxiality X_Σ for different initial porosities $f_0 = 0.1, 1, 5\%$ and Lode parameters: (a) $L = -1$, (b) $L = -0.5$, (c) $L = 0$ and (d) $L = 1$. Overall, an effect is observed especially near the transition from the low- to the high-triaxiality regimes, which becomes less sharp with decreasing porosity. It should also be noted that higher initial porosities f_0 lead to a reduction in ductility, as determined by the limit load, except in the transition regime, where the opposite trend is observed. Finally, Fig. 14 presents LOE critical curves as
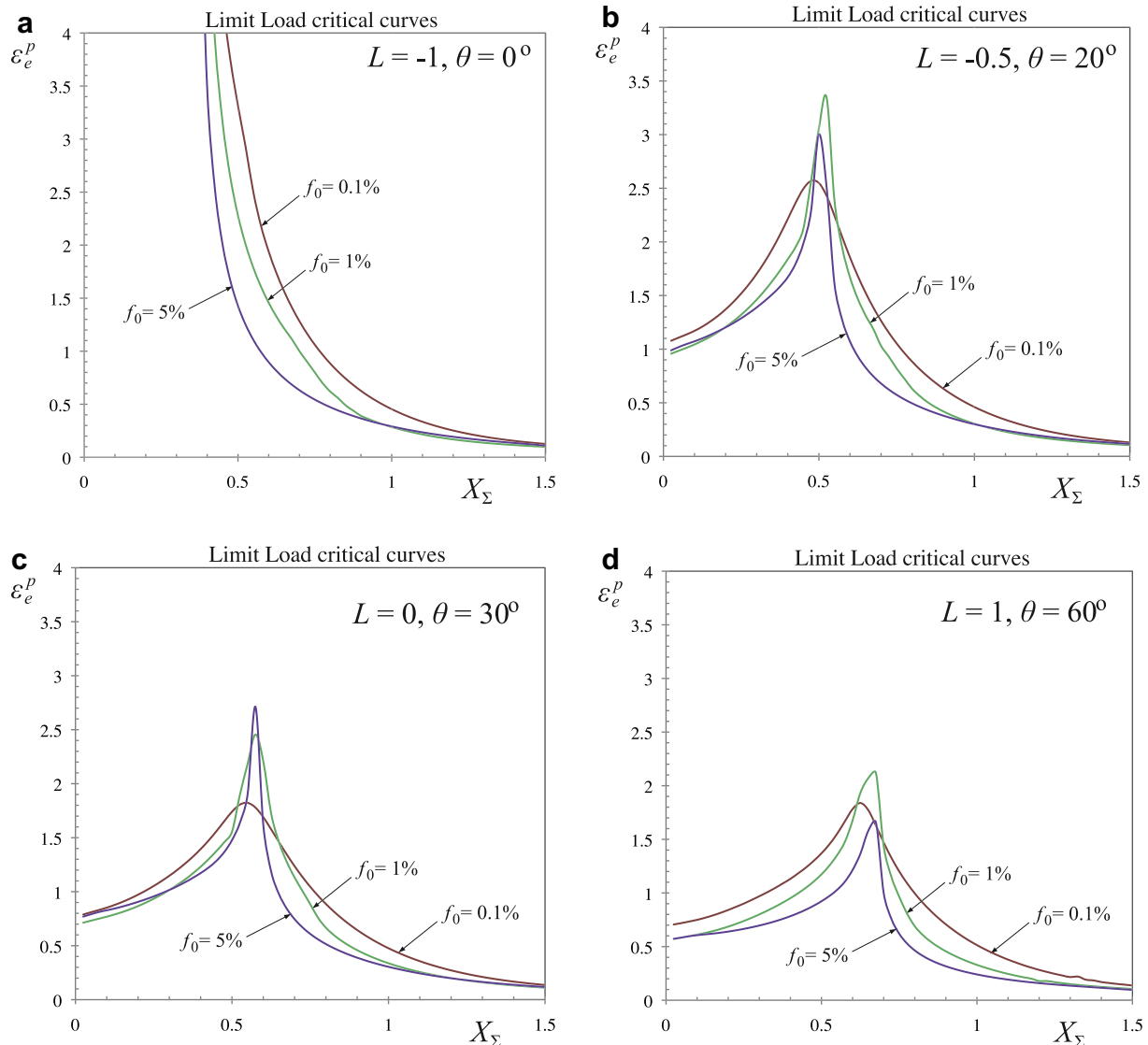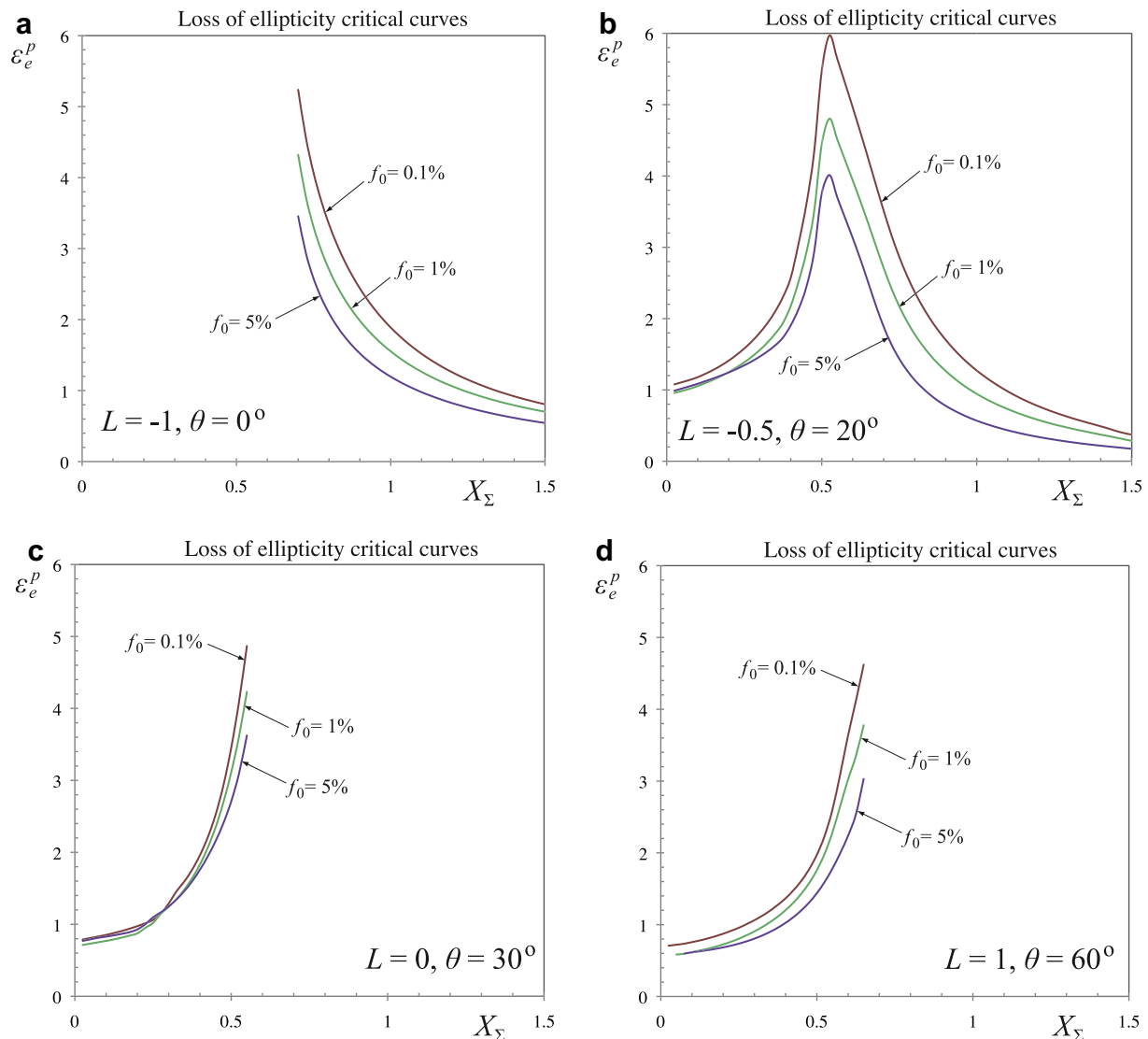

Fig. 13. SOM limit load failure curves as a function of the stress triaxiality X_Σ and the initial porosity $f_0 = 0.1, 15\%$ for various values of the Lode parameter: (a) $L = 1$, (b) $L = -0.5$, (c) $L = 0$ and (d) $L = 1$. The strain hardening exponent is $N = 0.1$.

Fig. 14. SOM loss of ellipticity failure curves as a function of the stress triaxiality X_Σ and the initial porosity $f_0 = 0.1, 15\%$ for various values of the Lode parameter: (a) $L = 1$, (b) $L = -0.5$, (c) $L = 0$ and (d) $L = 1$. The strain hardening exponent is $N = 0.1$.

a function of the stress triaxiality X_Σ for different initial porosities $f_0 = 0.1, 1$, and 5% and Lode parameters: (a) $L = -1$, (b) $L = -0.5$, (c) $L = 0$ and (d) $L = 1$. The effect of f_0 on the LOE failure curves is non-negligible contrary to the effect of the strain hardening exponent N shown in Fig. 12. As observed here, higher initial porosity f_0 leads to lower critical strains for localization, at least for the range of porosities considered in this study.

4. Conclusions and perspectives

In this work, we have investigated the influence of the stress triaxiality and the Lode parameter on the failure of elasto-plastic porous materials subjected to macroscopically uniform, triaxial loadings. For this purpose, we have made use of a recently developed "second-order" nonlinear homogenization model (SOM) of Danas and Ponte Castañeda (2009a), which can account for the effects of void shape and porosity evolution on the overall softening/hardening response of the porous material. Material failure of the porous ductile solid has been modeled by means of two different macroscopic criteria: (i) vanishing of the overall hardening rate ($H = 0$), corresponding to the existence of limit load, or maximum

stress in the constitutive response of the material, and (ii) loss of ellipticity of the incremental response of the material corresponding to localization of the deformation into dilatant shear bands due to the compressible overall response of the porous material (Rice, 1976).

The main finding of this work is that failure can occur by two very different mechanisms at high- and low-triaxiality. In agreement with well-established results, at high triaxialities, the model predicts significant *void growth* leading to a softening effect which eventually overtakes the intrinsic strain hardening of the solid material and produces overall softening. Thus, a limit load is reached at a critical strain that decreases with increasing triaxiality and is found to be independent of the Lode parameter. This limit load point is then followed by a significant reduction in the load-carrying capacity of the material and loss of ellipticity (at least for negative values of the Lode parameter). On the other hand, at low triaxialities, the model predicts *void collapse* due to an abrupt flattening of the initially spherical voids with *decreasing* porosity, which in turn leads to a sharp drop in the load-carrying capacity of the porous solid. The precise value of the strain at the onset of the instability, which determines the overall ductility of the material, depends on the competition of the hardening produced by the

reduction of the porosity and the softening due to the change in shape of the pores, and is highly sensitive to the value of the Lode parameter. Thus, for biaxial tension with axisymmetric compression ($L = 1$), the onset of the limit load instability, as well as the loss of ellipticity shortly thereafter, decreases as the triaxiality is reduced toward zero, while for axisymmetric tension ($L = -1$) no void collapse is possible and therefore no instability is observed for small values of the triaxiality. Moreover, for fixed, small values of the triaxiality ($X_\Sigma < 0.6$), the ductility of the porous material decreases as the value of the Lode parameter increases from -1 to $+1$. In addition, a sharp transition is observed as the failure mechanism switches from void collapse to void growth for intermediate values of the stress triaxiality ($0.3 < X_\Sigma < 0.7$), depending strongly on the value of the Lode parameter and leading to high-ductility peaks in the failure maps. In this regard, the theoretical predictions are found to be in qualitative agreement with recent experimental observations by Barsoum and Faleskog (2007a) and Dunand and Mohr (2010), even though it should be emphasized that the stress and deformation fields are not uniform and that the values of the triaxiality and Lode parameter are not controlled independently in these experiments. In this sense, the theoretical predictions presented in this work suggest the critical need for new experiments with improved control over the uniformity of the stress and strain fields, as well as the loading conditions.

The predictions of the second-order model have been compared with the corresponding results of the *ad hoc* modification of the Gurson model, MGUR, proposed by Nahshon and Hutchinson (2008), and significant differences have been identified. First and foremost, the MGUR model cannot capture void collapse, because the voids are assumed to remain spherical throughout the deformation. Because of this, while it is possible to artificially soften the material response by introducing a dependence on the Lode angle, the failure curves still increase with decreasing triaxiality into the negative triaxiality regime. In addition, in contrast with the second-order predictions, the effect of the Lode parameter on the maximum load is symmetric with respect to the sign of the Lode angle, and does not lead to loss of ellipticity for most values of the Lode parameter in the low-triaxiality regime. In this connection, it is important to emphasize that the relevance of the Lode angle is not so much through its direct effect on the macroscopic yield surface, which is relatively small, but instead through its much more significant implications for the evolution of the microstructure, especially when changes in the shape of the voids are allowed. Indeed, this ability to account for the very different and generally strongly anisotropic evolution of the microstructure of the material at fixed, low values of the stress triaxiality, but with different Lode parameters ranging from axisymmetric tension ($L = +1$) to biaxial tension with axisymmetric compression ($L = -1$), is the main advantage of the SOM model over the models of Gurson (1977), Nahshon and Hutchinson (2008) and Nielsen and Tvergaard (2010).

For completeness, the SOM model has also been used to investigate the possible effects of the matrix strain-hardening exponent N and the initial porosity f_0. We have found that the strain-hardening exponent N has a significant effect on the limit load for stress triaxialities $X_\Sigma > 0.4$, and consequently the location of the transition from the void collapse to the void growth mechanisms. In contrast, it has only a negligible effect on the limit load at low stress triaxialities, due to the abruptness of the void collapse mechanism in this case, leading to strong material softening. On the other hand, the strain hardening exponent affects only slightly the loss of ellipticity curves. In turn, different initial porosities f_0 have an effect on both the limit load and loss of ellipticity failure curves. Higher initial porosities lead, in general, to lower critical strains for the limit load and loss of ellipticity, except for the limit load curves in the transition region ($0.4 < X_\Sigma < 0.6$), where the opposite trend is observed.

It should also be emphasized that this work deals only with instabilities at the material level and that no actual macroscopic geometries have been considered. Nonetheless, the instability results obtained assuming that macroscopically uniform fields are present in a given specimen should correspond to "material instabilities," and provide a loose upper bound for the resistance of the material to ductile failure under more general loading conditions (Rice, 1976). In this connection, it is also relevant to mention that the three-dimensional studies of Barsoum and Faleskog (2007b) and Barsoum and Faleskog (2011) and the corresponding two-dimensional studies of Tvergaard (2009) in two-dimensions, seem to suggest that void rotations may somehow be necessary for low-triaxiality failure. However, the results of the present work for triaxial loading conditions (with fixed loading axes) show that while void rotations may enhance (or reduce) the ductility of the material, void rotations are not strictly necessary for material instabilities (of the maximum load, or loss of ellipticity type) at low-triaxiality, since the basic micro-mechanism of void collapse does not require them. In any event, void rotations can easily be handled by the general version of the SOM model (Danas and Ponte Castañeda, 2009a), and this will be pursued in future work. Interestingly, Kailasam and Ponte Castañeda (1997) have shown (refer to Fig. 2 in that reference) using an earlier version of the model (Ponte Castañeda and Zaidman, 1994; Kailasam and Ponte Castañeda, 1998) that the effective hardening rate of a porous rigid-plastic material subjected to simple shear can become zero as a consequence of the combined effects of the changes in shapes and orientation of the voids.

It should also be remarked that the larger issue of how to proceed after (local) loss of ellipticity in the analysis of an actual structural problem is still a largely open issue. However, it is clear that more general and reliable models, as well as estimates for their loss of ellipticity, are essential for further progress, as are finite element implementations of such models in order to be able to handle the non-uniform fields that would be expected to develop under actual experimental conditions. In this latter connection, it should be mentioned that such implementations are already available (see Kailasam et al. (2000) and Aravas and Ponte Castañeda (2004)) for the earlier "variational" framework of Ponte Castañeda and Zaidman (1994). In addition, a numerical implementation of an improved version of the "variational" framework, which provides more accurate results for both low and high stress triaxialities has been developed—and implemented for three-dimensional experimental geometries—recently by Danas and Aravas (2012).

As a final remark, it should be mentioned that an additional advantage in the use of a homogenization approach for porous and other heterogeneous solids is its generality. Thus, for example, the effect of anisotropy in the matrix can be accounted for in a straightforward fashion by treating this phase as a polycrystalline aggregate and using the second-order homogenization method (Liu and Ponte Castañeda, 2004) consistently to estimate the overall response including both the effects of porosity and crystallographic texture. A first step in this direction is presented in the recent work of Lebensohn et al. (2011), which opens up the possibility of modeling the simultaneous effects of porosity and texture evolution on the overall response and stability of porous polycrystalline solids, which is expected to be especially important for porous low-symmetry metals, such as porous Ti and Mg alloys.

It is also relevant to mention in this connection that the second-order homogenization method has been used successfully to estimate loss of ellipticity in porous elastomers (Lopez Pamies and Ponte Castañeda, 2007a,b). Although the failure maps are very different for this case, comparisons with careful numerical calculations (Michel et al., 2007) show that the model indeed has the capability of capturing not only the overall macroscopic behavior, but also the possible onset of "macroscopic" instabilities, such as loss of ellipticity (Geymonat et al., 1993).

Acknowledgments

References

Aravas, N., Ponte Castañeda, P., 2004. Numerical methods for porous metals with deformation-induced anisotropy. Comput. Methods Appl. Mech. Eng. 193, 3767–3805.

Bao, Y., Wierzbicki, T., 2004. On fracture locus in the equivalent strain and stress triaxiality space. Int. J. Mech. Sci. 46 (81), 81–98.

Barsoum, I., Faleskog, J., 2007a. Rupture mechanisms in combined tension and shearExperiments. Int. J. Solids Struct. 44, 1768–1786.

Barsoum, I., Faleskog, J., 2007b. Rupture mechanisms in combined tension and shearMicromechanics. Int. J. Solids Struct. 44, 5481–5498.

Barsoum, I., Faleskog, J., 2011. Micromechanical analysis on the influence of the Lode parameter on void growth and coalescence. Int. J. Solids Struct. 48, 925–938.

Benzerga, A.A., 2002. Micromechanics of coalescence in Ductile fracture. J. Mech. Phys. Solids 50, 1331–1362.

Benzerga, A.A., Leblond, J.-B., 2010. Ductile fracture by void growth to coalescence. Adv. Appl. Mech. 44, 170–297.

Benzerga, A.A., Besson, J., Pineau, A., 1999. Coalescence-controlled anisotropic Ductile fracture. J. Eng. Mater. Tech. 121, 221–229.

Budiansky, B., Hutchinson, J.W., Slutsky, S., 1982. Void Growth and Collapse in Viscous Solids. In: Hopkins, H.G., Sewell, M.J. (Eds.), Mechanics of Solids, The Rodney Hill 60th Aniversary Volume. Pergamon Press, Oxford, pp. 13–45.

Chu, C.C., Needleman, A., 1980. Void nucleation effects in biaxially stretched sheets. J. Eng. Mat. Tech. 102, 249–256.

Dafalias, Y.F., 1985. The plastic spin. J. Appl. Mech. 52, 865–871.

Danas, K., 2008. Homogenization-based constitutive models for viscoplastic porous media with evolving microstructure. Ph.D. thesis, LMS, École Polytechnique: http://www.polymedia.polytechnique.fr/Center.cfm?Table=These.

Danas, K., Aravas, N., 2012. Numerical modeling of elasto-plastic porous materials with void shape effects at finite deformations. Composites Part B, http://dx.doi.org/10.1016/j.compositesb.2011.12.011.

Danas, K., Ponte Castañeda, P., 2009a. A finite-strain model for anisotropic viscoplastic porous media I - Theory. Eur. J. Mech. A Solids 28, 387–401.

Danas, K., Ponte Castañeda, P., 2009b. A finite-strain model for anisotropic viscoplastic porous media: II - Applications. Eur. J. Mech. A Solids 28, 402–416.

Danas, K., Idiart, M.I., Ponte Castañeda, P., 2008a. A homogenization-based constitutive model for two-dimensional viscoplastic porous media. C.R. Mecanique 336, 79–90.

Danas, K., Idiart, M.I., Ponte Castañeda, P., 2008b. A homogenization-based constitutive model for isotropic viscoplastic porous media. Int. J. Solids Struct. 45, 3392–3409.

Dunand, M., Mohr, D., 2010. Hybrid experimental-numerical analysis of basic ductile fracture experiments for sheet metals. Int. J. Solids Struct. 47, 1130–1143.

Duva, J.M., Hutchinson, J.W., 1984. Constitutive potentials for dilutely voided nonlinear materials. Mech. Mater. 3, 41–54.

Eshelby, J.D., 1957. The determination of the elastic field of an ellipsoidal inclusion and related problems. Proc. R. Soc. Lond. A 241, 376–396.

Flandi, L., Leblond, J.-B., 2005. A new model for porous nonlinear viscous solids incorporating void shape effects - I: Theory. Eur. J. Mech. A Solids 24, 537–551.

Gărajeu, M., Michel, J.-C., Suquet, P., 2000. A micromechanical approach of damage in viscoplastic materials by evolution in size shape and distribution of voids. Comp. Methods Appl. Mech. Eng. 183, 223–246.

Garrison Jr., W.M., Moody, N.R., 1987. Ductile fracture. J. Phys. Chem. Solids 48, 1035–1074.

Geymonat, G., Müller, S., Triantafyllidis, N., 1993. Homogenization of nonlinearly elastic materials microscopic bifurcation and macroscopic loss of rank-one convexity. Arch. Ration. Mech. Anal. 122, 231–290.

Gologanu, M., Leblond, J.-B., Devaux, J., 1993. Approximate models for ductile metals containing non-spherical voids – case of axisymmetric prolate ellipsoidal cavities. J. Mech. Phys. Solids 41, 1723–1754.

Gologanu, M., Leblond, J.-B., Devaux, J., 1994. Approximate models for ductile metals containing non-spherical voids – case of axisymmetric oblate ellipsoidal cavities. ASME J. Eng. Mater. Tech. 116, 290–297.

Gologanu, M., Leblond, J.-B., Devaux, J., 1997. Recent Extensions of Gurson's Model for Porous Ductile Metals. In: Suquet, P. (Ed.), Continuum Micromechanics, CISM Lectures Series. Springer, New York, pp. 61–130.

Gurson, A.L., 1977. Continuum theory of ductile rupture by void nucleation and growth. J. Eng. Mater. Tech. 99, 2–15.

Hancock, J.W., Mackenzie, A.C., 1976. On the mechanisms of ductile fracture in high-strength steels subject to multi-axial stress-states. J. Mech. Phys. Solids 24, 147–160.

Johnson, G.R., Cook, W.H., 1985. Fracture characteristics of three metals subjected to various strains, strain rates, temperatures and pressures. Eng. Fract. Mech. 21 (1), 31–48.

Kailasam, M., Ponte Castañeda, P., 1997. The Evolution of Anisotropy in Porous Materials and its Implications for Shear Localization. In: Fleck, N.A., Cocks, A.C.F. (Eds.), IUTAM Symposium on Mechanics of Granular and Porous Materials. Kluwer Academic Publishers, pp. 365–376.

Kailasam, M., Ponte Castañeda, P., 1998. A general constitutive theory for linear and nonlinear particulate media with microstructure evolution. J. Mech. Phys. Solids 46, 427–465.

Kailasam, M., Ponte Castañeda, P., Willis, J.R., 1997a. The effect of particle size, shape, distribution and their evolution on the constitutive response of nonlinearly viscous composites I. Theory. Phil. Trans. R. Soc. Lond. 355, 1835–1852.

Kailasam, M., Ponte Castañeda, P., Willis, J.R., 1997b. The effect of particle size, shape, distribution and their evolution on the constitutive response of nonlinearly viscous composites II. Examples. Phil. Trans. R. Soc. Lond. A 355, 1853–1872.

Kailasam, M., Aravas, N., Ponte Castañeda, P., 2000. Porous metals with developing anisotropy: constitutive models, computational issues and applications to deformation processing. Comput. Model. Eng. Sci 1, 105–118.

Keralavarma, S.M., Benzerga, A.A., 2010. A constitutive model for plastically anisotropic solids with non-spherical voids. J. Mech. Phys. Solids 58, 874–901.

Lebensohn, R.A., Idiart, M.I., Ponte Castañeda, P., Vincent, P.-G., 2011. Dilatational viscoplasticity of polycrystalline solids with intergranular cavities. Phil. Mag. 91, 3038–3067.

Lee, B.J., Mear, M.E., 1992. Axisymmetric deformation of power-law solids containing a dilute concentration of aligned spheroidal voids. J. Mech. Phys. Solids 40, 1805–1836.

Le Roy, G., Embury, J.D., Edwards, G., Ashby, M.F., 1981. A model of Ductile fracture based on the nucleation and growth of voids. Acta Met. 29, 1509–1522.

Liu, Y., Ponte Castañeda, P., 2004. Second-order theory for the effective behavior and field fluctuations in viscoplastic polycrystals. J. Mech. Phys. Solids 52, 467–495.

Lopez Pamies, O., Ponte Castañeda, P., 2007a. Homogenization-based constitutive models for porous elastomers and implications for macroscopic instabilities: I Analysis. J. Mech. Phys. Solids 55, 1677–1701.

Lopez Pamies, O., Ponte Castañeda, P., 2007b. Homogenization-based constitutive models for porous elastomers and implications for macroscopic instabilities: II Results. J. Mech. Phys. Solids 55, 1702–1728.

McClintock, F.A., 1968. A criterion for by Ductile fracture by growth of holes. Trans. ASME Ser. E J. Appl. Mech. 35, 363–371.

McClintock, F.A., 1971. Plasticity aspects of fracture. In: Leibowitz, H. (Ed.), Fracture, vol. 3. Academic Press, pp. 47–225.

Michel, J.-C., Suquet, P., 1992. The constitutive law of nonlinear viscous and porous materials. J. Mech. Phys. Solids 40, 783–812.

Michel, J.-C., Lopez-Pamies, O., Ponte Castañeda, P., Triantafyllidis, N., 2007. Microscopic and macroscopic instabilities in finitely strained porous elastomers. J. Mech. Phys. Solids 55, 900–938.

Mohr, D., Ebnoether, F., 2009. Plasticity and fracture of martensitic boron steel under plane stress conditions. Int. J. Solids Struct. 46, 3535–3547.

Monchiet, V., Charkaluk, E., Kondo, D., 2007. An improvement of Gurson-type models of porous materials by using Eshelby-like trial velocity fields. C.R. Mcanique 335, 32–41.

Nahshon, K., Hutchinson, J.W., 2008. Modification of the Gurson model for shear failure. Eur. J. Mech. A Solids 27, 1–17.

Needleman, A., Rice, J.R., 1978. Limits to ductility set by plastic flow localization. In: Koistinen, D.P. et al. (Eds.), Mechanics of Sheet Metal Forming. Plenum, Publishing, pp. 37–267.

Nielsen, K.L., Tvergaard, V., 2010. Ductile shear failure or plug failure of spot welds modelled by modified Gurson model. Eng. Fract. Mech. 77, 1031–1047.

Pardoen, T., Hutchinson, J.W., 2000. An extended model for void growth and coalescence. J. Mech. Phys. Solids 48, 2467–2512.

Ponte Castañeda, P., 1991. The effective mechanical properties of nonlinear isotropic composites. J. Mech. Phys. Solids 39, 45–71.

Ponte Castañeda, P., 2002a. Second-order homogenization estimates for nonlinear composites incorporating field fluctuations I. Theory. J. Mech. Phys. Solids 50, 737–757.

Ponte Castañeda, P., 2002b. Second-order homogenization estimates for nonlinear composites incorporating field fluctuations II. Applications. J. Mech. Phys. Solids 50, 759–782.

Ponte Castañeda, P., Willis, J.R., 1995. The effect of spatial distribution on the effective behavior of composite materials and cracked media. J. Mech. Phys. Solids 43, 1919–1951.

Ponte Castañeda, P., Zaidman, M., 1994. Constitutive models for porous materials with evolving microstructure. J. Mech. Phys. Solids 42, 1459–1497.

Rice, J.R., 1976. The localization of plastic deformation. In: Koiter, W.T.,(Ed.) Proceedings of the 14th International Congress of Theoretical and Applied Mechanics, North-Holland Publishing Company, pp. 207–220.

Rice, J.R., Tracey, D.M., 1969. On the ductile enlargement of voids in triaxial fields. J. Mech. Phys. Solids 17, 201–217.

Teirlinck, D., Zok, F., Embury, J.D., Ashby, M.F., 1988. Fracture mechanism maps in stress space. Acta Met. 36 (5), 1213–1228.

Tvergaard, V., 1981. Influence of voids on shear band instabilities under plane strain conditions. Int. J. Fract. 17, 389–407.

Tvergaard, V., 1990. Material failure by void growth. Adv. Appl. Mech. 27, 83–151.

Tvergaard, V., 2009. Behaviour of voids in a shear field. Int. J. Fract. 158, 41–49.

Willis, J.R., 1978. Variational principles and bounds for the overall properties of composites. Contin. Models Discrete Syst. 2, 185–212.

Willis, J.R., 1981. Variational and related methods for the overall properties of composites. Adv. Appl. Mech. 21, 1–78.

Willis, J.R., 1991. On methods for bounding the overall properties of nonlinear composites. J. Mech. Phys. Solids 39, 73–86.

Yamamoto, H., 1978. Conditions for shear localization in the ductile fracture of void containing materials. Int. J. Fract. 14, 347–365.